Strathprints Institutional Repository

Open Source DSMC Chemistry Modelling for Hypersonic Flows

Thomas J. Scanlon[1*], Craig White[1], Matthew K. Borg[1], Rodrigo C. Palharini[1], Erin Farbar[2], Iain D. Boyd[2], Jason M. Reese[3] and Richard E. Brown[4]

[1]*James Weir Fluids Laboratory, Department of Mechanical and Aerospace Engineering, University of Strathclyde, Glasgow G1 1XJ, UK*

[2]*Department of Aerospace Engineering, University of Michigan, 48109-2140, USA*

[3] *School of Engineering, University of Edinburgh, Edinburgh EH9 3HL, UK*

[4]*Centre for Future Air-Space Transportation Technology, Department of Mechanical and Aerospace Engineering, University of Strathclyde, Glasgow G1 1XJ, UK*

Abstract

An open source implementation of chemistry modelling for the direct simulation Monte Carlo (DSMC) method is presented. Following the recent work of Bird [1] an approach known as the quantum kinetic (Q-K) method has been adopted to describe chemical reactions in a 5-species air model using DSMC procedures based on microscopic gas information. The Q-K technique has been implemented within the framework of the *dsmcFoam* code, a derivative of the open source CFD code OpenFOAM. Results for vibrational relaxation, dissociation and exchange reaction rates for an adiabatic bath demonstrate the success of the Q-K model when compared with analytical solutions for both inert and reacting conditions. A comparison is also made between the Q-K and total collision energy (TCE) chemistry approaches for a hypersonic flow benchmark case.

---

* Contact author: tom.scanlon@strath.ac.uk

1.   Introduction

Hypersonic vehicles, which typically operate in rarefied gas environments, are subject to extremes of velocity and altitude. So it is important that the aerodynamic and thermal loads on the vehicle are properly characterised if the feasibility of the vehicle design is to be accurately assessed. The vehicle may also encounter chemical reactions that can have a significant influence on aerodynamic performance and vehicle surface heat flux [2]. Numerical models that fail to incorporate such reacting flows miss an essential part of the flow physics surrounding the vehicle.

The planetary atmospheres through which hypersonic vehicles may pass consist of a number of chemical species, the relative proportion of which varies with altitude. Although the gas in the atmosphere is composed, at the microscopic level, of discrete atoms and molecules, a useful approximation arises if the atmosphere is treated as a continuum. The flow over a vehicle moving through the atmosphere can then be modelled by appealing to the fundamental principles of momentum interchange and mass and energy conservation. This continuum approach is at the root of conventional computational fluid dynamics (CFD) methods for the solution of the Navier-Stokes-Fourier (NSF) equations. Indeed, continuum CFD has been applied successfully in many simulations of gas flow around air- and spacecraft, and yields good agreement with measured data over a wide range of practically-relevant operational conditions [3].

However, continuum-based models have limitations in rarefied gas conditions. The extent of gas rarefaction is traditionally gauged by the Knudsen number, *Kn*, defined as the ratio of the mean free path of the gas molecules to a characteristic length scale of the vehicle. As the Knudsen number increases, the non-continuum, particulate-like behaviour of the gas becomes more important. Numerical models hoping to simulate such rarefied conditions must be able capture the complex physics shown in figure 1

for high-speed vehicle re-entry. The flow environment is characterised by a distinct bow-shock upstream of the body with a high temperature region immediately downstream of the shock. In this searingly hot region, chemical reactions may take place involving dissociation, exchange and ionization, while surface chemistry is also possible. In the wake of the craft there is a highly rarefied zone within which thermochemical non-equilibrium conditions may exist. The paucity of molecules in this zone may necessitate the region being described using a non-continuum, particle-based formulation.
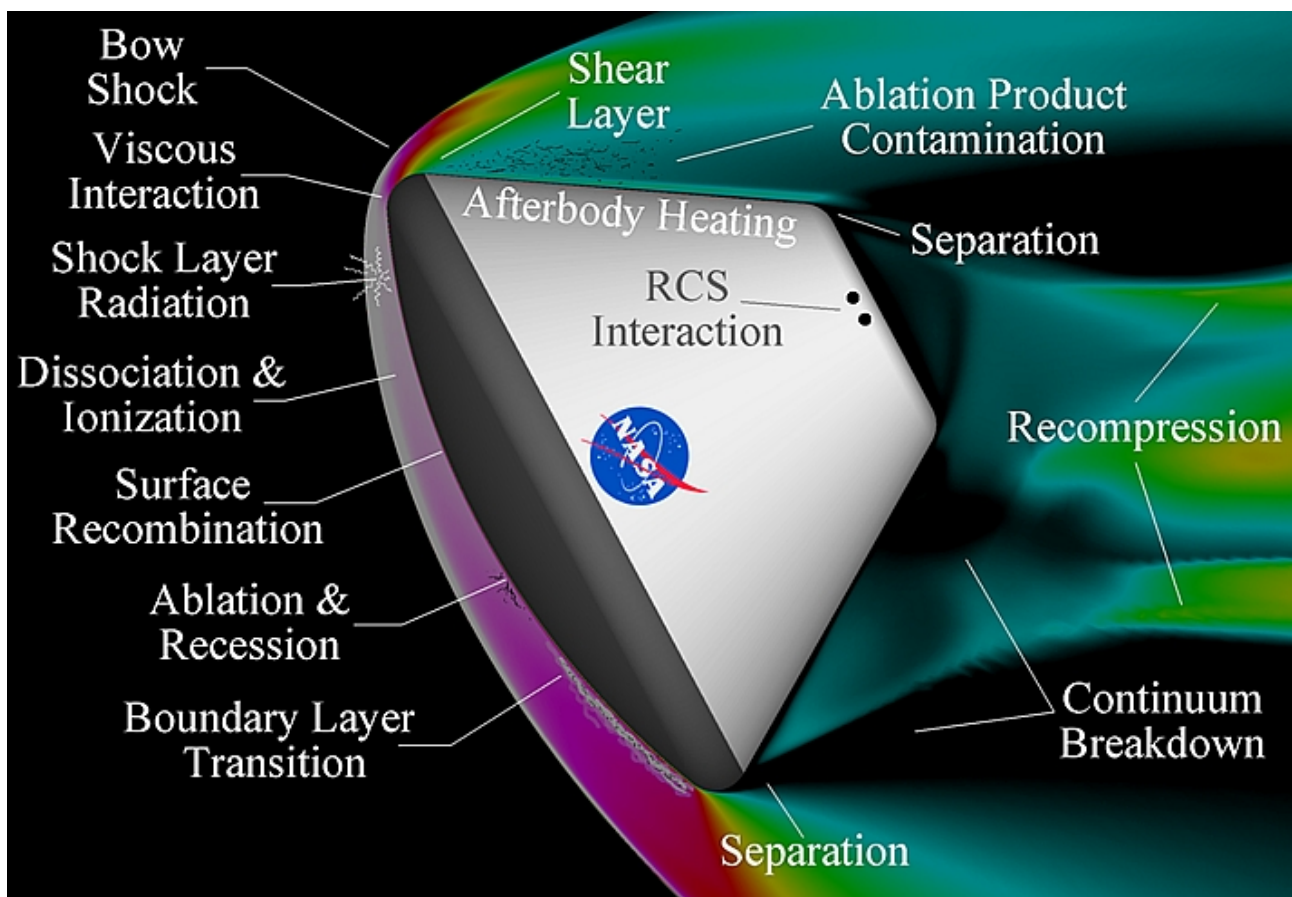

Figure 1 *Complex physics in planetary vehicle re-entry* (*image credit NASA*).

It may be possible to describe such complex flow conditions using the Boltzmann equation, which is appropriate for the entire range of Knudsen numbers likely to be encountered by hypersonic vehicles. However, the Boltzmann equation is extremely

difficult to solve numerically due to its high dimensionality and the complexity of the collision term. Simplification of the collision term in the equation through the Bhatnagar–Gross–Krook (BGK) approximation [4] has given rise to a number of new numerical algorithms, such as the model Boltzmann equation (MBE) solver developed by Yang and Huang [5]; however these nascent techniques have yet to establish themselves as practical simulation tools, particularly for high-speed reacting flows.

The problem that the conventional Navier-Stokes-Fourier (NSF) equations have in capturing rarefaction is highlighted in figure 2 [6]. The normal shock wave is a fundamental component of many high-speed aerodynamic flows, e.g. in the central
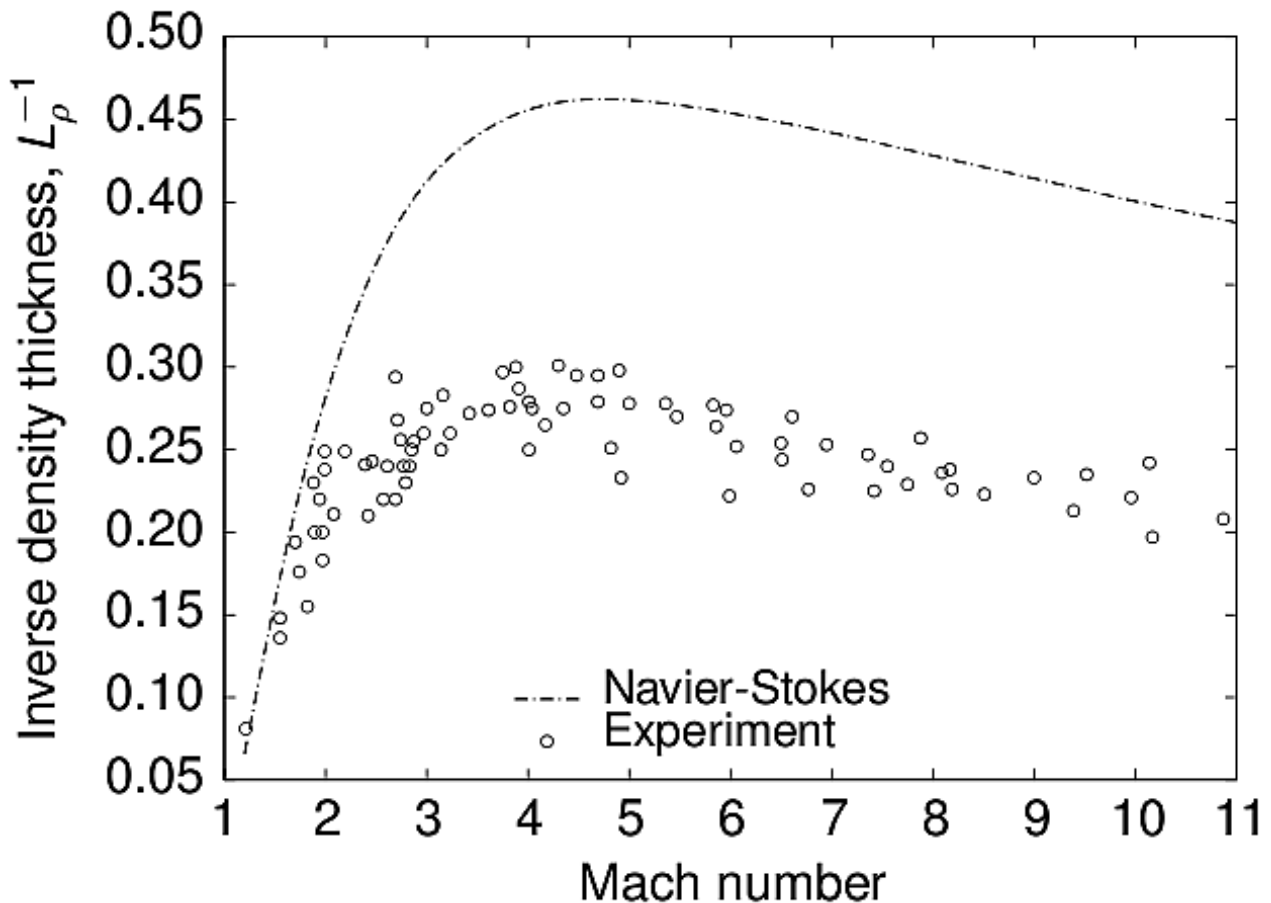

Figure 2 *The inverse of the normalised density thickness of normal shock waves in argon gas up to Mach 11.*

4

part of the bow shock. Rarefaction causes the shock to be relatively thick (of the order of a few gas mean-free-paths - of the same order as the stand-off distance of the bow shock from the vehicle leading edge). This figure shows that the NSF equations consistently predict shocks in argon gas that are some 50% thinner than observed experimentally. That the fluid dynamic equations have such difficulty in predicting the behaviour in such a simple flow case, calls their appropriateness for more complex rarefied flow fields into question.

Non-continuum behaviour can be accommodated to some extent in conventional NSF approaches to modelling the gas dynamics around aero-space vehicles, for instance by incorporating a finite slip velocity between the gas and any solid surfaces that are immersed within the flow. A computationally-efficient gas flow method, but one which has had only modest success to date, is to establish either a *Kn*-series or a Hermite polynomial approximation to the molecular velocity distribution function in the Boltzmann equation. To first order (i.e. for near-equilibrium flows) this approach yields the NSF set, but the solution method can be continued to second and higher orders to incorporate more and more of the salient characteristics of a rarefied flow. This family of so-called extended hydrodynamic equations has various different members, including the Burnett, Grad 13-moment, R13, R26 equations, and others. Generally, they all have great difficulty in achieving stable physical solutions of high-Mach-number flows. Their non-linearity also makes them difficult to solve numerically and, as they are higher-order in the gradients of flow properties, their solution requires additional boundary conditions that are not easy to define. For these reasons, extended hydrodynamics has not established a firm place in the armoury of tools a high-speed aerodynamicist can deploy.

1.1 *The Direct Simulation Monte Carlo (DSMC) method*

In highly rarefied environments ($Kn > 0.1$) accommodation of the thermochemical non-equilibrium effects that occur in the flow away from surfaces remains a challenging problem. For this reason, analysis of gas flows in the non-continuum regime is most naturally conducted using specialised computational techniques that are derived from a statistical mechanical representation of the behaviour of the individual particles comprising the flow. The most successful of these techniques is undoubtedly the direct simulation Monte Carlo (DSMC) approach, originally proposed by Bird [7].

The DSMC technique instructs particles to move and collide using kinetic-theory considerations that can capture the non-continuum gas behaviour accurately. DSMC considers molecular collisions using stochastic rather than deterministic procedures over a time step which is a small fraction of the mean collision time, and each DSMC particle represents a large number of real gas molecules. The decoupling of particle ballistic motion and particle collisions improves the computational efficiency of DSMC greatly in comparison with other particle methods such as molecular dynamics (MD). The computational domain is divided into either a structured or unstructured grid of cells, with each cell of a dimension that is a small fraction of the local mean free path. The cells are then utilised to select particles for collisions on a probabilistic basis, and also are used for sampling the macroscopic flow properties. Intermolecular collisions are handled probabilistically using phenomenological models that are designed to reproduce real fluid behaviour when the flow is examined at the macroscopic level. The DSMC technique has been shown to provide a solution to the Boltzmann equation as the number of simulated particles tends toward infinity [8]. The DSMC approach is currently the dominant numerical method for rarefied gas flow applications.

1.2 *Thermochemistry effects*

For engineering purposes, the gas in the Earth's atmosphere may be assumed to be a binary mixture of oxygen (O_2) and nitrogen (N_2). In the DSMC methodology, particle clusters must be endowed with the correct properties to capture kinetic and rotational modes of energy storage. Vibrational excitation of the gas molecules as well as dissociation of both oxygen and nitrogen are likely to be important features of the flow around any hypersonic vehicle at the highest altitudes (80-120 km) and speeds, while even at lower speeds and altitudes vibrational excitation and limited dissociation of oxygen are still likely to be important [9]. Such real-gas effects need to be properly accounted for. The DSMC technique normally models air as either a 5-species mixture using dissociation, recombination and exchange reactions, or as a mixture of 11-species including ionisation. In conventional CFD, reaction rates are calculated according to the Arrhenius law [9]. However, this relies on data sourced from equilibrium conditions, which may be inappropriate for rarefied hypersonic flows. In contrast, the DSMC method, with its particulate approach, is able to capture successfully the thermochemical non-equilibrium effects encountered in high speed rarefied gas environments [1, 2].

2. Chemistry modelling in *dsmcFoam*

The DSMC code used for this paper is called *dsmcFoam*. The code has been written within the framework of the open source C++ CFD toolbox OpenFOAM [10]. The main features of the *dsmcFoam* code include the capability to perform both steady and transient DSMC simulations for multi-species conditions, to model arbitrary 2D/3D geometries using unstructured polyhedral meshes, and unlimited parallel processing. The original version of *dsmcFoam* determines intermolecular collisions for polyatomic species using the variable hard sphere (VHS) model and applies the phenomenological Larsen-Borgnakke model to distribute post-collision energy between the translational and rotational modes [7]. A series of successful benchmark

trials have been carried out to verify the *dsmcFoam* code for non-reacting flows [11].

2.1 *Vibrational energy and the Q-K chemistry model*

The vibrational energy mode plays a key role in chemical reactions using the Q-K model. This mode was excluded in previous versions of *dsmcFoam* [11] so this section describes the implementation and validation of the vibrational mode into the code. The vibrational modes of a gas are generally active when the system is sufficiently energised, e.g. under the high enthalpy conditions commonly found in hypersonic applications. The vibrational mode forms part of the total energy budget and limits the amount of post-collision energy available to the translational and rotational modes. In addition, it often introduces a new mode of non-equilibrium to a rarefied gas system as the number of collisions required for vibrational relaxation is significantly higher than that for translational or rotational equilibration.

For the implementation of the vibrational mode in *dsmcFoam* it is proposed that the vibrational energy can only assume discrete quantum values, as described by Haas *et al.* [12] and Bergman and Boyd [13]. We consider a serial application of the quantum Larsen-Borgnakke method using the harmonic oscillator model to redistribute vibrational energy before rotational and translational energy exchange are considered. It is desirable in DSMC to avoid the use of the macroscopic temperature whenever possible as colliding particles have no knowledge of the surrounding temperature. Here, we discuss a model for the redistribution of vibrational energy based on the collision energy (as opposed to the local macroscopic temperature of the gas). The first step is to define a "quantized collision temperature", T_{coll}, based on the collision energy of a particle pair, p and q, [14]:

$$T_{coll} = \frac{i_{max}\theta_v}{\frac{7}{2} - \omega} \quad , \tag{1}$$

where

$$i_{max} = \lfloor \frac{E_c}{k\theta_v} \rfloor \quad , \tag{2}$$

and $\lfloor ... \rfloor$ denotes truncation, i_{max} is the maximum quantum level available to the molecule, θ_v is the vibrational temperature, k is the Boltzmann constant, ω is the temperature exponent of viscosity, and E_c is the sum of the relative translational energy of the collision pair and the pre-collision vibrational energy of the molecule under consideration, i.e.

$$E_c = \varepsilon_{tr,pq} + \varepsilon_{v,p} \quad . \tag{3}$$

The vibrational collision number Z_v can then be calculated as [14]

$$Z_v = \left(\frac{\theta_d}{T_{coll}}\right)^{\omega} \left[Z_{ref} \left(\frac{\theta_d}{T_{Z_{ref}}}\right)^{-\omega} \right]^{\left[\left(\frac{\theta_d}{T_{coll}}\right)^{\frac{1}{3}} - 1 \right] / \left[\left(\frac{\theta_d}{T_{Z_{ref}}}\right)^{\frac{1}{3}} - 1 \right]} \quad , \tag{4}$$

where θ_d is the characteristic dissociation temperature and Z_{ref} is the vibrational collision number at a reference temperature T_{zref}, which is usually taken to be the characteristic vibrational temperature, θ_v , such that [15],

$$Z_{ref} = \left(\frac{C_1}{T_{Z_{ref}}^{\omega}}\right) \exp\left(C_2 T_{Z_{ref}}^{-1/3}\right), \tag{5}$$

where C_1 and C_2 are constants which can be found in Appendix A of Ref [7], and T_{Zref}

is set as θ_v .

Once the vibrational collision number has been calculated, the particle is tested for vibrational energy exchange and is accepted if

$$\frac{1}{Z_v} > R_f \ ,$$

(6)

where R_f is a random number between 0 and 1. An integer post-collision vibrational quantum level i^* is chosen uniformly between 0 and the maximum possible level i^*_{max} and the acceptance-rejection method is used to select a value of i^* using a quantized version of the Larsen-Borgnakke probability ratio [13]:

$$\frac{P}{P_{max}} = \left(1 - \frac{i^* k \theta_v}{E_c}\right).$$

(7)

The total energy of the pair is reduced accordingly, and particle p is then considered for relaxation into the rotational and translational modes using the standard Larsen-Borgnakke approach.

In order to verify the implementation of this vibrational energy exchange, a test case involving relaxation to equilibrium is considered. This test case involves an adiabatic box filled with nitrogen gas, in a similar manner to that considered by Bird [16]. The translational and rotational temperatures are initially 20,000 K and there is no energy in the vibrational mode. The reference vibrational collision number Z_{ref} is 19.8 at a reference temperature of 20,000 K. The *dsmcFoam* simulation is performed using the VHS collision model, with the following properties ascertained at T_{ref} = 273 K: $m = 46.5 \times 10^{-27}$ kg, $\omega = 0.74$ and $d_{ref} = 4.17 \times 10^{-10}$ m, where d_{ref} and m are the

10

molecular diameter and mass, respectively.

The cell is filled with 1.2 million DSMC particles and, as the particles begin to collide, energy is transferred to the vibrational mode and equipartition is achieved at a temperature of around 14,720 K after a period of relaxation, as shown in Figure 3. The 'collision number' on the abscissa is calculated as the product of the instantaneous collision rate from the simulation and the physical time that has elapsed. The *dsmcFoam* results agree well with those of Bird's DS2V code [16]. The rotational temperature follows the translational temperature closely and the vibrational temperature takes a longer time to arrive at equilibrium. The relaxation rates of all temperatures and the final equilibrium temperature are in good agreement with Bird's results.
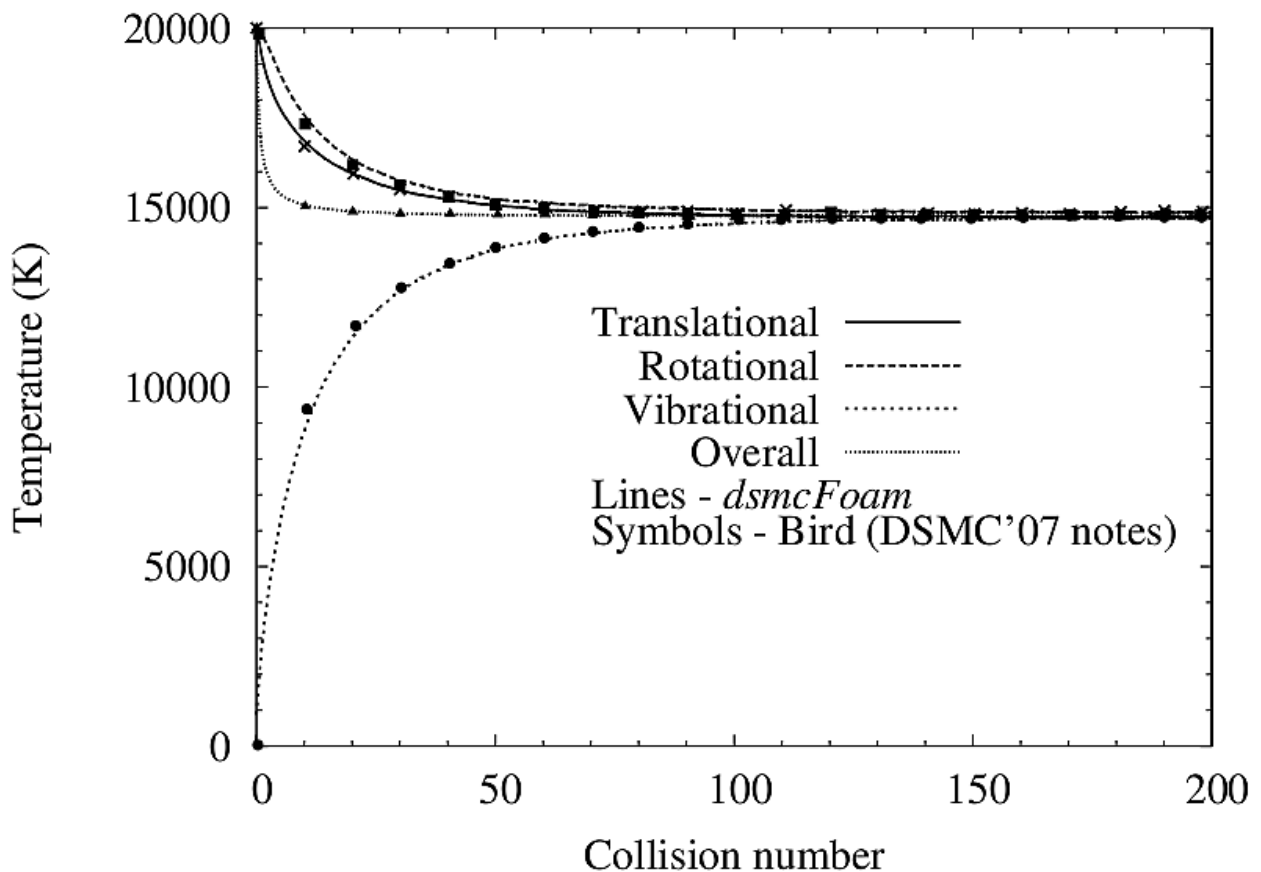
Figure 3 *Vibrational relaxation of nitrogen gas.*

2.2 *Quantum-kinetic chemical reactions*

Until recently, chemically reacting gas flows in DSMC have relied upon input data derived at the macroscopic level and reaction rate coefficients that are derived from equilibrium theory. This method for treating chemical reactions was introduced by Bird in 1979 and is known as the "total collision energy" (TCE) model [17]. The TCE chemical reaction model is well established and is used in mature DSMC codes such as MONACO [18].

As an alternative approach, Bird has recently proposed a chemical reaction model that is founded on the quantum Larsen-Borgnakke method described in section 2.1. This model has only a limited dependence on macroscopic data as the vibrational collision number is a function of the collision temperature (microscopic level) and a reference temperature (macroscopic level). The method also does not require that the gas be in a state near thermodynamic equilibrium. This is termed the "quantum-kinetic" (Q-K) model, and it has been developed over the past five years [1, 2, 14, 19].

In this paper we consider dissociation and exchange reactions using the Q-K approach with the aim of creating a five-species (oxygen O_2, nitrogen N_2, nitric oxide *NO*, atomic oxygen *O*, and atomic nitrogen *N*) air chemistry model for use in the open source *dsmcFoam* code.

2.3 *Dissociation reactions*

The condition for a dissociation reaction in the Q-K model is as follows: if the energy in a collision is high enough to allow a dissociation event, it will always occur. The reaction being considered is $AB + C \rightarrow A + B + C$, where *AB* is the molecule considered for dissociation, *C* is the reactant partner (either a molecule or an atom)

and *A* and *B* are the atomic products of the dissociation. Considering the serial application of the quantum Larsen-Borgnakke model, the collision energy E_c of a particle pair (*AB* + *C*) is the sum of the relative translational energy and the pre-collision vibrational energy of the particle currently being considered, as described by Equation (3). The maximum vibrational level that can be selected i_{max} is given by Equation (2). If i_{max} is beyond the dissociation limit, i.e.

$$i_{max} > \frac{\theta_d}{\theta_v} \quad , \tag{8}$$

then the molecule AB must be dissociated before any vibrational or rotational relaxation can be considered.

A distinct feature of the Q-K model is that although the DSMC implementation does not necessitate that the gas be in equilibrium, if it is assumed that it is, then analytical solutions for the reaction rates can be derived. For a VHS gas in equilibrium, the rate coefficient $k_f(T)$ for the dissociation of a molecule *AB* with a molecule or atom *C* is

$$k_f(T) = R_{coll}^{AB,C} \gamma (i_{max})^{AB,C}, \tag{9}$$

where $R_{coll}^{AB,C}$ is the collision rate between species *AB* and *C* divided by the number density product. For an equilibrium VHS gas, this is

$$R_{coll}^{AB,C} = \frac{2\pi^{1/2}}{\alpha} (r_{ref}^{AB} + r_{ref}^{C})^2 \left(\frac{T}{T_{ref}} \right)^{1-\omega^{AB,C}} \left(\frac{2kT_{ref}}{m_r^{AB,C}} \right)^{1/2}, \tag{10}$$

where r_{ref}, T_{ref} and ω are the standard VHS properties of the relevant gas species, m_r is the reduced mass of the collision pair, and *T* is the macroscopic temperature of the gas. The symmetry factor α is set to 2 if the molecules in the collision are identical or 1 for dissimilar molecules. The $\gamma(i_{max})^{AB,C}$ parameter defines the fraction of collisions that will have sufficient energy to dissociate. Taking *i* as the pre-collision vibrational state of the dissociating molecule, the result is

$$y(i_{max})^{AB,C} = \sum_{i=0}^{i_{max}-1} \frac{1}{z_v(T)^{AB}} \left[Q\left(\frac{5}{2} - \omega^{AB,C}, \left(\frac{(i_{max}-i)\theta_v^{AB}}{T} \right) \right) \exp\left(\frac{-i\,\theta_v^{AB}}{T} \right) \right], \qquad (11)$$

where $Q(a, x) = \Gamma(a, x) / \Gamma(a)$ is a form of the incomplete Gamma function and $z_v(T)^{AB} = 1/[1 - \exp(-\theta_v/T)]$ is the vibrational partition function [1].

2.3.1 *Dissociation in dsmcFoam*

We have implemented Q-K dissociation reactions in *dsmcFoam* for the following nine molecule-molecule dissociations, which we term "Type I" dissociations:

$$O_2 + O_2 \rightarrow O + O + O_2, \qquad (12)$$

$$N_2 + N_2 \rightarrow N + N + N_2, \qquad (13)$$

$$NO + NO \rightarrow N + O + NO, \qquad (14)$$

$$O_2 + N_2 \rightarrow O + O + N_2, \qquad (15)$$

$$N_2 + O_2 \rightarrow N + N + O_2, \qquad (16)$$

$$O_2 + NO \rightarrow O + O + NO, \qquad (17)$$

$$N_2 + NO \rightarrow N + N + NO, \qquad (18)$$

$$NO + O_2 \rightarrow N + O + O_2, \qquad (19)$$

$$NO + N_2 \rightarrow N + O + N_2, \qquad (20)$$

and the following six molecule-atom dissociations, or "Type II" dissociations

$$O_2 + O \rightarrow O + O + O, \qquad (21)$$

$$O_2 + N \rightarrow O + O + N, \qquad (22)$$

$$N_2 + O \rightarrow N + N + O, \qquad (23)$$

$$N_2 + N \rightarrow N + N + N, \qquad (24)$$

$$NO + O \rightarrow N + O + O, \tag{25}$$

$$NO + N \rightarrow N + O + N. \tag{26}$$

We consider dissociation reactions for two cases involving either thermochemical equilibrium or non-equilibrium. For the case of equilibrium, if a DSMC particle meets the criterion for dissociation to occur (Equation 8) then we may simply update a counter within our DSMC simulation during which no particle splitting takes place. This procedure enables reaction rates to be calculated at a constant temperature for a gas in equilibrium and then compared to the analytical Q-K solution of Equation (9). In his 2011 Q-K paper [1], Bird does not present any DSMC simulation data: it is solely analytical work with a description of the DSMC procedure for each reaction. Gallis *et al*. [2] and Wysong *et al*. [19] have presented some DSMC simulation data, however this work was performed using a DSMC implementation for exchange reactions that has since been superseded.

For the non-equilibrium case, particle splitting may occur and nascent species are introduced with the associated conservation of mass, momentum and energy. This procedure gives rise to an initial non-equilibrium mixture which eventually settles down to steady-state, thermochemical equilibrium. For the non-equilibrium case the results from the *dsmcFoam* Q-K implementation are compared with analytical solutions. The analytical results are generated for the simultaneous solution of rate kinetic equations describing the time evolution of the concentration of each chemical species as well as the equilibrium temperature of the reacting gas mixture [20]. The overall rate of change of the concentration of species *s* is given by the summation over all individual rate processes of the form:

$$\frac{d[X_s]}{dt} = -k_f[X_s][X_r] + k_b[X_{p1}][X_{p2}], \tag{27}$$

where k_f and k_b are forward and backward rate coefficients, X_r is a reactant species, and X_{p1} and X_{p2} are product species. The forward reaction only is considered and backward recombination is deactivated. The k_f is determined from the equilibrium Q-K rate (Equation 9) and is set in Arrhenius form as shown in Table 1. A system of five equations is solved simultaneously for species N_2, O_2, NO, N, and O for high-temperature air. The overall energy balance is also analysed accounting for the internal energy modes (translation, rotation, vibration) and chemical reactions in order to determine the equilibrium temperature.

2.3.2 *Equilibrium dissociation*

Adiabatic box simulations are performed to measure the equilibrium dissociation rate coefficients for each reaction. A single cubic cell of side length 1×10^{-5} *m*, with six specularly reflective surfaces, was used for this purpose. Following the work of Haas [21], a total of 50,000 DSMC particles were used in each simulation, a time step size of 1.52×10^{-9} *s* was adopted, and the rotational and vibrational collision numbers were set to 1. The particles were allowed to move and exchange energy but no particle splitting occurred. Only the forward reaction was considered during the reaction, and recombination was discounted.

Figure 4 shows the Type I equilibrium dissociation reaction rate coefficient for the dissociation of oxygen in collisions with another oxygen molecule. Good agreement is found between the simulated and analytical Q-K rates (Equation 9). Comparison is also made with the DSMC results of Gallis *et al.* [2] for which excellent agreement is found, verifying the *dsmcFoam* implementation of the Q-K approach for dissociation. Finally, comparison with the TCE solution of Boyd [18] is made and reasonable concurrence is found, with Q-K predicting slightly higher rate coefficients across the range of temperatures considered.
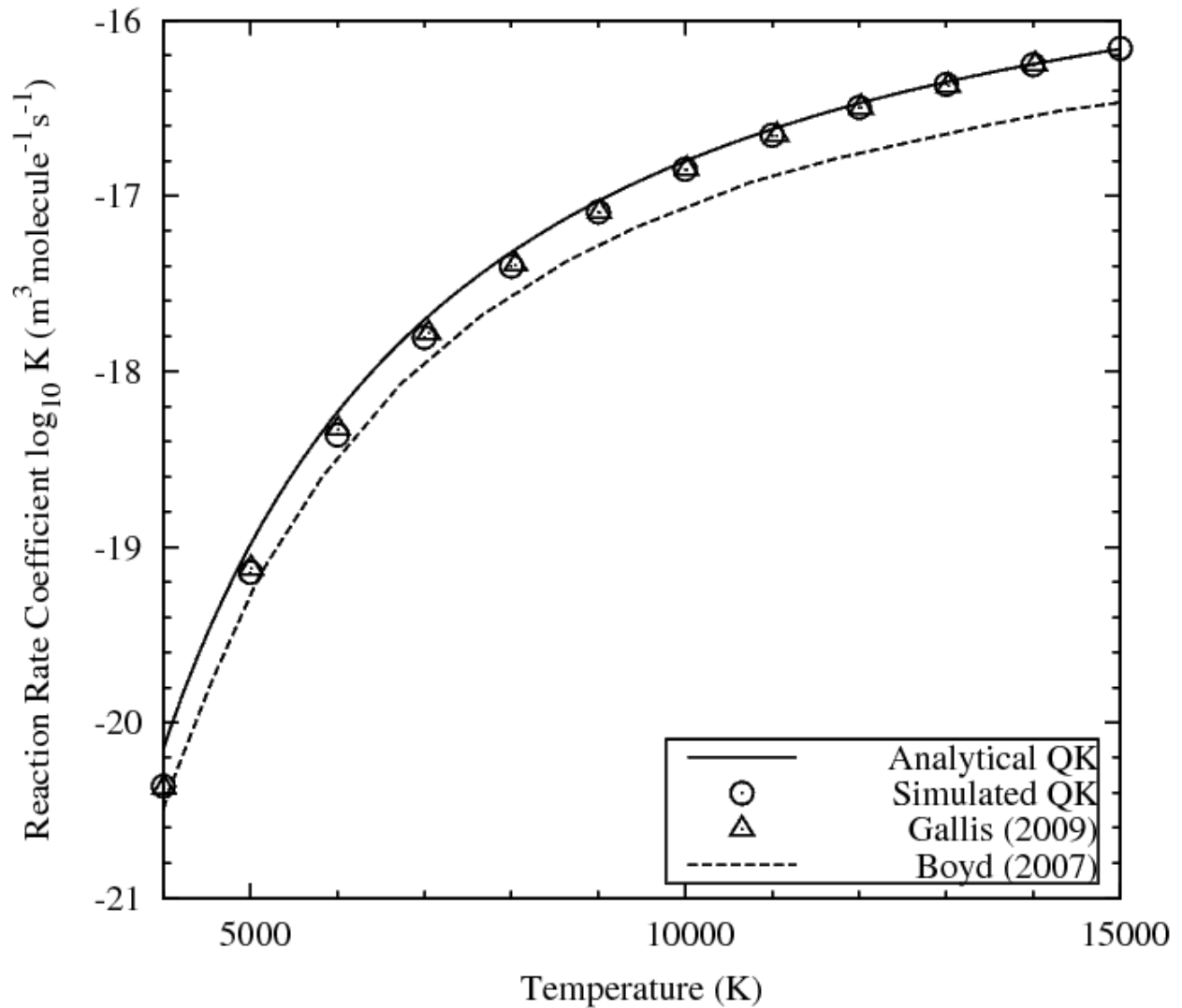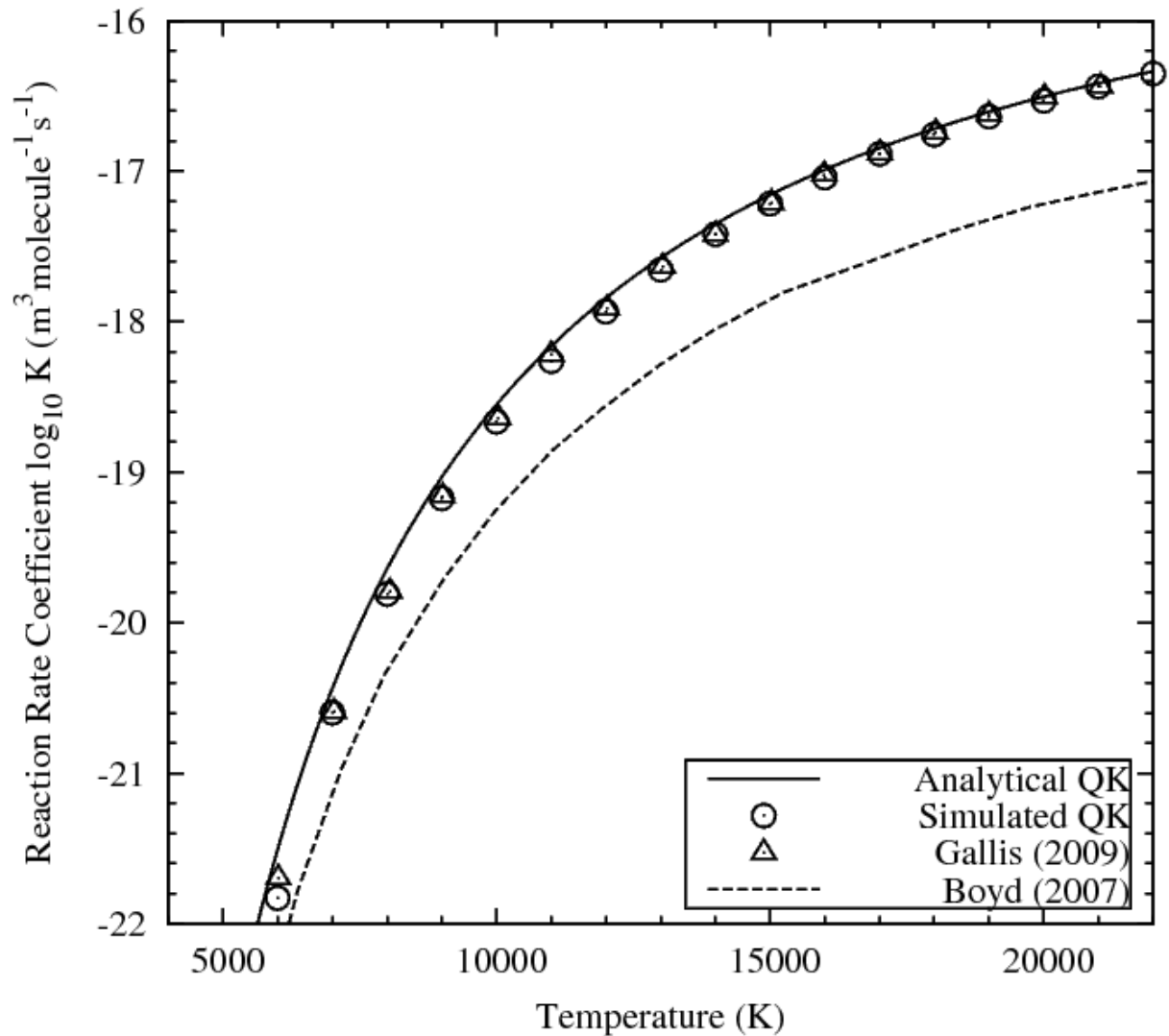
Figure 4 *Equilibrium dissociation rate coefficient for Type I dissociation,*

$$O_2+O_2 \rightarrow O+O+O_2.$$

Figure 5 shows the equilibrium reaction rate coefficients for the Type I dissociation reaction defined by Equation (13), i.e. dissociation of a nitrogen molecule in a collision with another nitrogen molecule. The analytical and numerical Q-K solutions are again in satisfactory agreement, while the *dsmcFoam* Q-K values remain in excellent agreement with those of Gallis *et al*. [2]. In comparison with the TCE [18] results the Q-K values show a similar trend, however the level of agreement is not as close as with the oxygen reaction and higher Q-K values are predicted once again.

Figure 5 *Equilibrium dissociation rate coefficient for Type I dissociation,*

$$N_2 + N_2 \rightarrow N + N + N_2 .$$

Figures 6 and 7 show the equilibrium rate coefficients for the Type II dissociations described by Equations (21) and (24). Excellent agreement is found between the analytical Q-K, simulated Q-K and the Gallis *et al.* DSMC results [2], while satisfactory agreement is achieved with the TCE rates of Boyd [18]. Although not presented in this paper for reasons of conciseness, the remaining Type I and Type II dissociation reactions have been implemented in *dsmcFoam* and these demonstrate similar levels of agreement to those shown in Figures 4 to 7 when compared with the
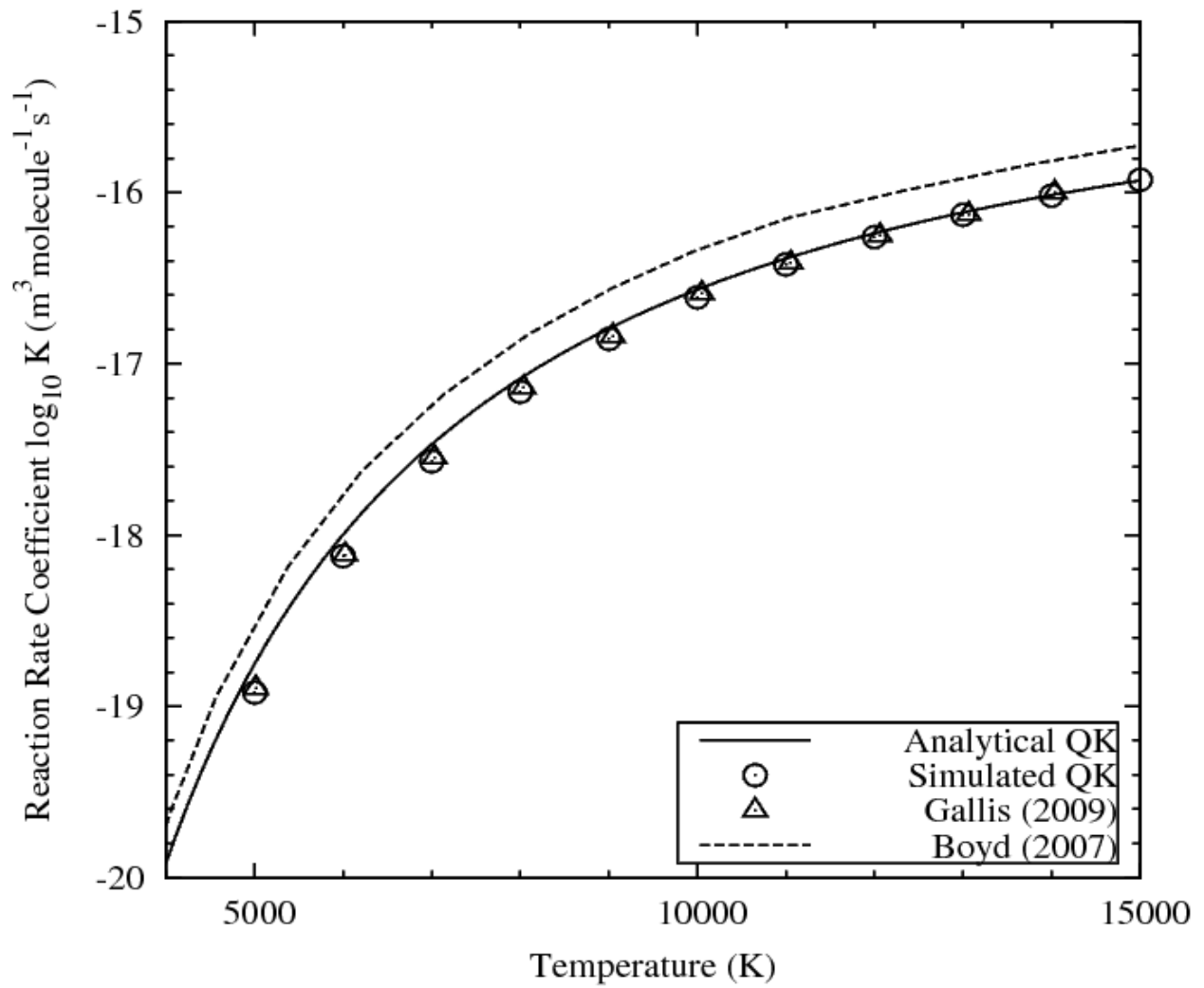
Figure 6 *Equilibrium dissociation rate coefficient for Type II dissociation,*

$$O_2 + O \rightarrow O + O + O.$$

Q-K analytical rates, the Gallis *et al*. [2] DSMC results and Boyd's [18] TCE rates.
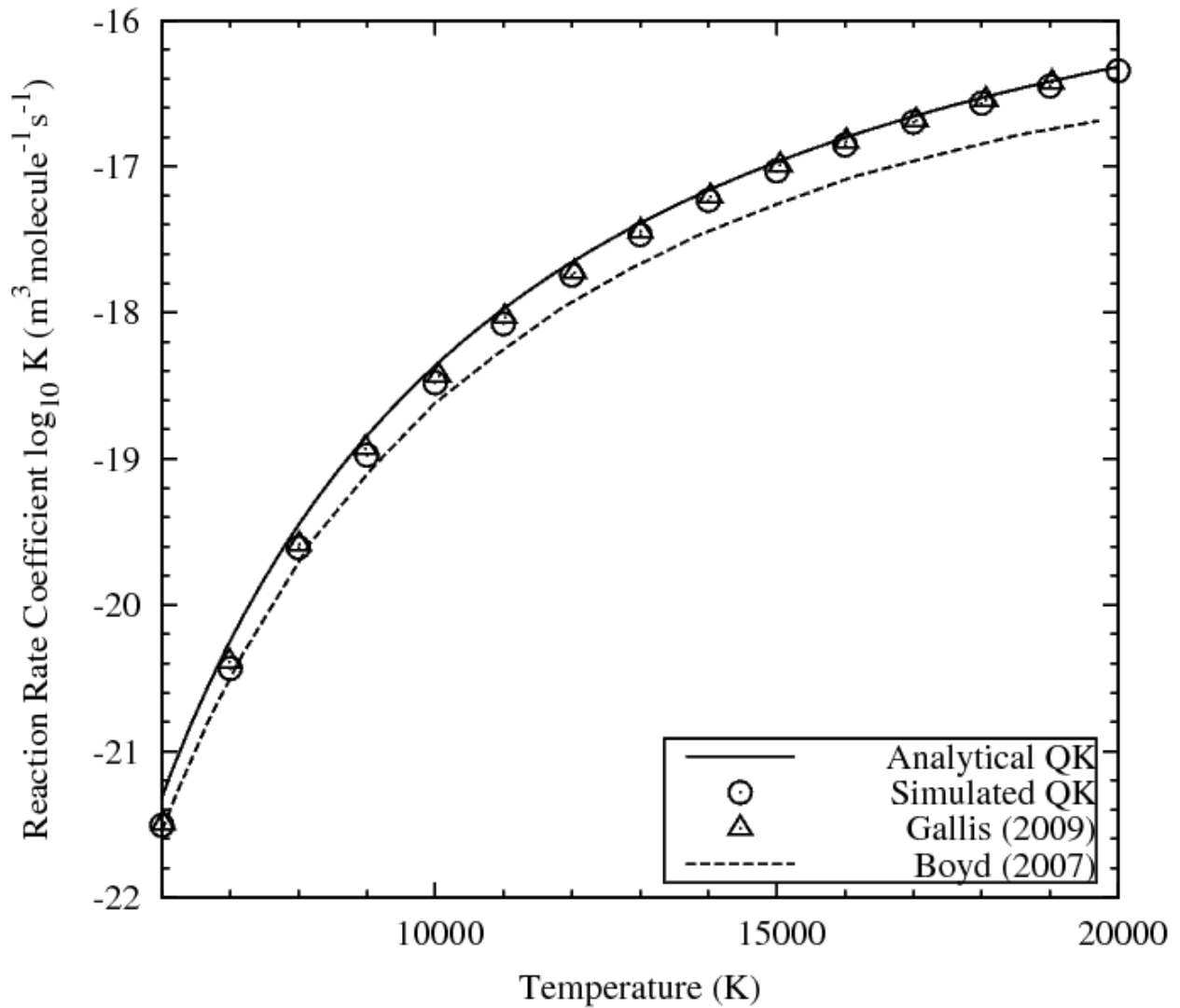
Figure 7 *Equilibrium dissociation rate coefficient for Type II dissociation*

$$N_2 + N \rightarrow N + N + N.$$
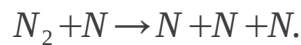
2.3.3 *Non-equilibrium dissociation*

Unlike the equilibrium rate calculations shown previously, the non-equilibrium dissociation reactions described in this section involve particle splitting. The physical dissociation of the molecules is accompanied by a process of detailed balance for mass, momentum and energy as DSMC particles disintegrate. A single cell adiabatic cube of side length 1×10^{-5} *m* is again employed, and 50,000 initial DSMC particles

were used with a time-step of 1.52×10^{-9} *s*. The fate of each species is measured in a transient manner as the reaction proceeds from equilibrium initial conditions, through a non-equilibrium reaction process to a final state approaching equilibrium. Once again, the backward recombination reaction has been deactivated and only the forward chemistry is dealt with. For internal energy exchange both the rotational and vibrational collision numbers have been fixed at 1. The *dsmcFoam* Q-K results are compared with the analytical solution provided by Equation (27). The forward rate coefficient $k_f(T)$ for Equation (27) is provided as a best-fit Arrhenius curve to the equilibrium analytical Q-K data given by Equation (9), while the Arrhenius rate takes the form:

$$k_f(T) = C_1 T^{(C_2)} \exp\left(\frac{-E_a}{kT}\right), \tag{28}$$

where k is the Boltzmann constant, C_1 and C_2 are reaction-specific constants, and E_a is the activation energy, the values of which are provided in Table 1.

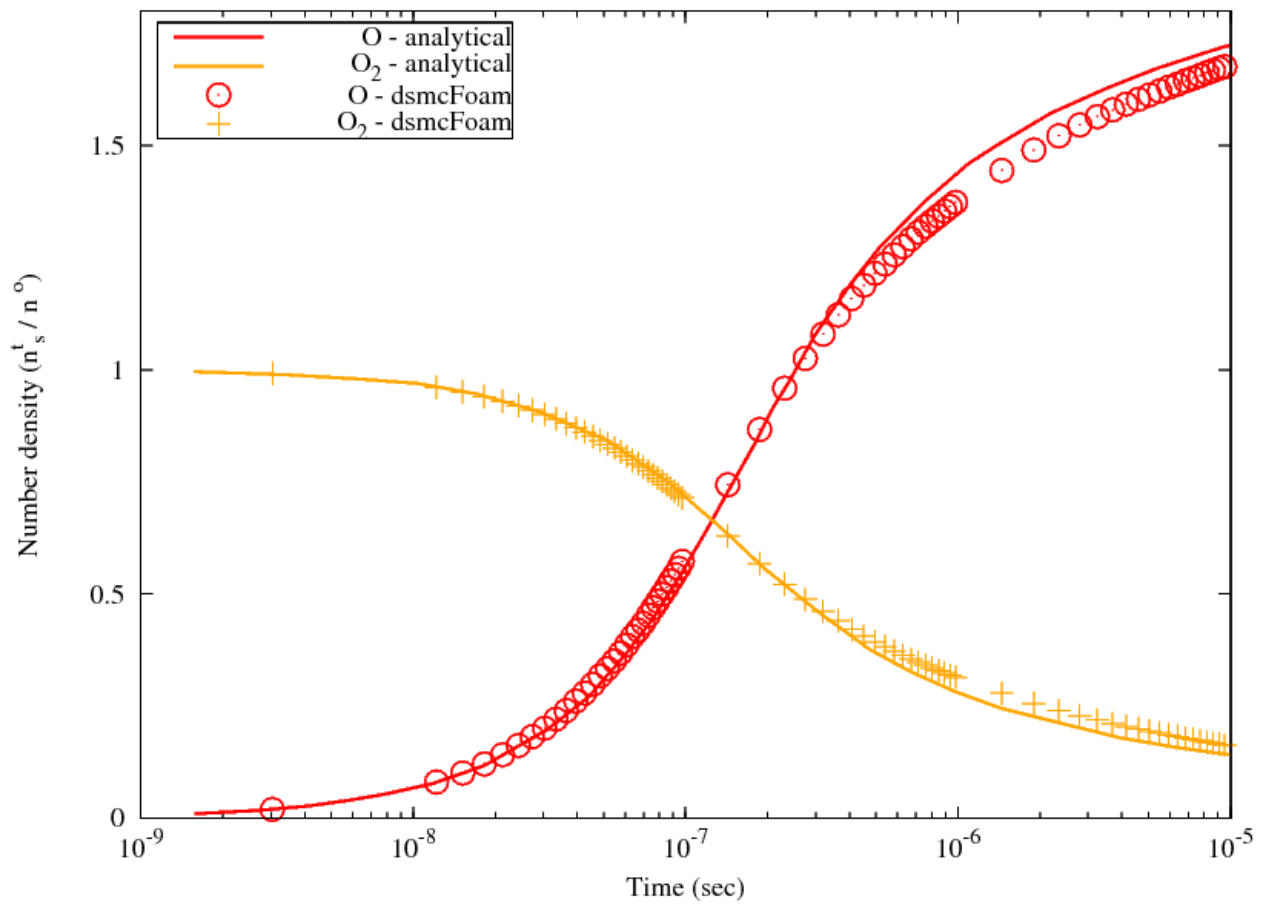Figure 8 shows the species concentrations during the dissociation of an O_2 reservoir from an initial temperature of 20,000 *K* and a pressure of 0.063 *atm*. Both Type I and Type II dissociations are activated (reaction numbers 4 and 5 in Table 1). The species concentrations at any instant in time (n_s^t) have been non-dimensionalised with respect to the the initial number density of the species (n^0). The analytical and numerical Q-K solutions seem to be in good agreement, with species constancy being approached after 10^{-5} *s*.

The transient temperature variation for the gas mixture is shown in Figure 9. Excellent concurrence is found with the analytical solution. Dissociation, being an endothermic reaction process, results in a temperature decline to a gas mixture temperature of approximately 6000 *K* after 10^{-5} *s*.

Table 1 *Chemical reaction list and equivalent Arrhenius rate variables for the 5-species air model in dsmcFoam.*

No.	Reaction	Heat of formation $\times 10^{19}$ J	C_1	C_2	Activation energy E_a $\times 10^{19}$ J
1	$O_2 + N \rightarrow O + O + N$	8.197	1.1×10^{-10}	-1.0	8.197
2	$O_2 + NO \rightarrow O + O + NO$	8.197	1.1×10^{-10}	-1.0	8.197
3	$O_2 + N_2 \rightarrow O + O + N_2$	8.197	1.3×10^{-10}	-1.0	8.197
4	$O_2 + O_2 \rightarrow O + O + O_2$	8.197	5.33×10^{-11}	-1.0	8.197
5	$O_2 + O \rightarrow O + O + O$	8.197	1.5×10^{-10}	-1.05	8.197
6	$N_2 + O \rightarrow N + N + O$	15.67	4.0×10^{-12}	-0.54	15.67
7	$N_2 + O_2 \rightarrow N + N + O_2$	15.67	1.5×10^{-11}	-0.68	15.67
8	$N_2 + NO \rightarrow N + N + NO$	15.67	1.5×10^{-11}	-0.68	15.67
9	$N_2 + N_2 \rightarrow N + N + N_2$	15.67	4.1×10^{-12}	-0.62	15.67
10	$N_2 + N \rightarrow N + N + N$	15.67	1.0×10^{-11}	-0.68	15.67
11	$NO + N_2 \rightarrow N + O + N_2$	10.43	2.1×10^{-10}	-1.0	10.43
12	$NO + O_2 \rightarrow N + O + O_2$	10.43	2.0×10^{-10}	-1.0	10.43
13	$NO + NO \rightarrow N + O + NO$	10.43	1.0×10^{-10}	-1.0	10.43
14	$NO + O \rightarrow N + O + O$	10.43	4.0×10^{-10}	-1.1	10.43
15	$NO + N \rightarrow N + O + N$	10.43	4.0×10^{-10}	-1.1	10.43
16	$NO + O \rightarrow O_2 + N$	2.719	2.3×10^{-19}	0.50	2.719
17	$N_2 + O \rightarrow NO + N$	5.175	0.8×10^{-16}	0	5.175
18	$O_2 + N \rightarrow NO + O$	-2.719	4.0×10^{-15}	-0.39	0.2
19	$NO + N \rightarrow N_2 + O$	-5.175	5.0×10^{-16}	-0.35	0.2

Figure 8 *Species concentrations during the dissociation of an O₂ reservoir from an initial temperature of 20,000 K and a pressure of 0.063 atm.*
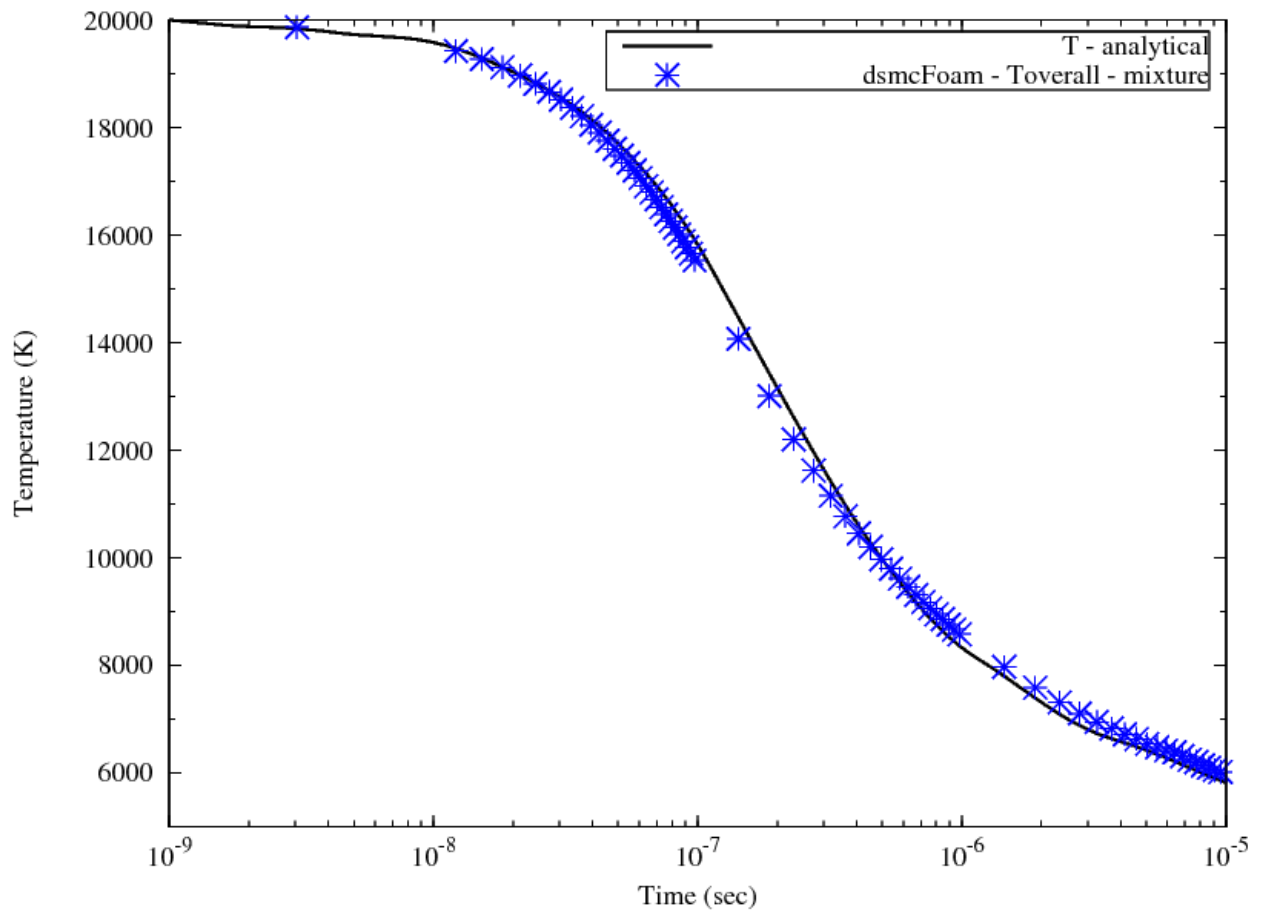
Figure 9 *Gas mixture overall temperature during the dissociation of an O₂ reservoir from an initial temperature of 20,000 K and a pressure of 0.063 atm.*

These results highlight the important role that endothermic dissociation plays in acting as an energy sink in hypersonic reacting flows. The energy redistribution during the chemical reaction manifests itself as a reduction in the enthalpy of the flow, with a consequent reduction in surface heat transfer to the hypersonic body.

2.4 *Exchange reactions*

An exchange reaction comprises one stable molecule and one radical before and after the reaction occurs. These reactions take the form $A+B \leftrightarrow C+D$, where A and C are molecules, and B and D are atoms. In the 5-species air model considered in this

paper, there are two sets of exchange reactions:

$$N_2 + O \leftrightarrow NO + N \,, \tag{29}$$

and

$$NO + O \leftrightarrow O_2 + N. \tag{30}$$

Each of these has a forward (endothermic) and a backward (exothermic) direction resulting in a total of four exchange reactions.

The DSMC implementation of exchange chemistry leads to reactions being possible if the collision energy E_c is greater than the activation energy E_a, with a probability of

$$P = \left(1 - \frac{E_a}{E_c}\right)^{3/2-\omega} \bigg/ \sum_{i=0}^{i_{max}} \left(1 - \frac{i k \theta_v}{E_c}\right)^{3/2-\omega} . \tag{31}$$

The summation in the denominator can be taken as unity when $E_a/k < \theta_v$ and the analytical Q-K rates given by Bird [1] are

$$k_f(T) = R_{coll}^{A,B} \exp\left(\frac{E_a^{A,B}}{kT}\right) \bigg/ z_v(T)^A \,, \tag{32}$$

and

$$k_r(T) = R_{coll}^{C,D} \exp\left(\frac{E_a^{C,D}}{kT}\right) \bigg/ z_v(T)^C \,, \tag{33}$$

where $k_f(T)$ and $k_r(T)$ are the forward and reverse reaction rates, respectively, $z_v(T)$ is the vibrational partition function, and R_{coll} is the collision rate between the species indicated in the superscript and is given by Equation (10).

The default activation energy for the forward exchange reactions is the heat of

reaction, E_r, and for the reverse reaction it is zero. The activation energies and heats of formation for the four exchange reactions are shown in Table 1 (reaction numbers 16 to 19).

In order to ensure that the ratio of the number of forward to reverse exchange reactions is consistent with that predicted by statistical mechanics it is necessary to adjust the activation energies in a phenomenological manner. For forward exchange reactions, the adjusted activation energy $E'_{a,f}$ is

$$E'_{a,f} = |E_h| \left[1 + a \left(\frac{T}{273} \right)^b \right],$$

(34)

and for the reverse exchange reaction it is

$$E'_{a,r} = |E_h| \left[a \left(\frac{T}{273} \right)^b \right],$$

(35)

where $|E_h|$ is the modulus of the heat of formation (see Table 1) and a and b are adjustable parameters.

Table 2 *Parameters for adjusted activation energies in Equations (34) and (35).*

Exchange reaction	a	b
$NO + O \rightarrow O_2 + N$	0.085	0.65
$O_2 + N \rightarrow NO + O$	0.1	0.1
$N_2 + O \rightarrow NO + N$	0.15	0.15
$NO + N \rightarrow N_2 + O$	0.033	0.8

In our *dsmcFoam* implementation, we have chosen values of a and b for the four exchange reactions that enable our DSMC results to be in satisfactory agreement with both the analytical equilibrium Q-K rates of Equations (32) and (33), and the analytical non-equilibrium rates predicted by Equation (27), and, finally, to ensure that the ratio of the forward to reverse reactions is consistent with that predicted by

statistical mechanics [1]. The parameters *a* and *b* are given in Table 2 and were determined using Bird's QKRates program [22]. Plots showing the ratio of forward to reverse exchange reaction rates are shown in Figures 10 and 11, and reasonable agreement is found for both exchange reactions in comparison with the equilibrium constant from statistical mechanics [22].
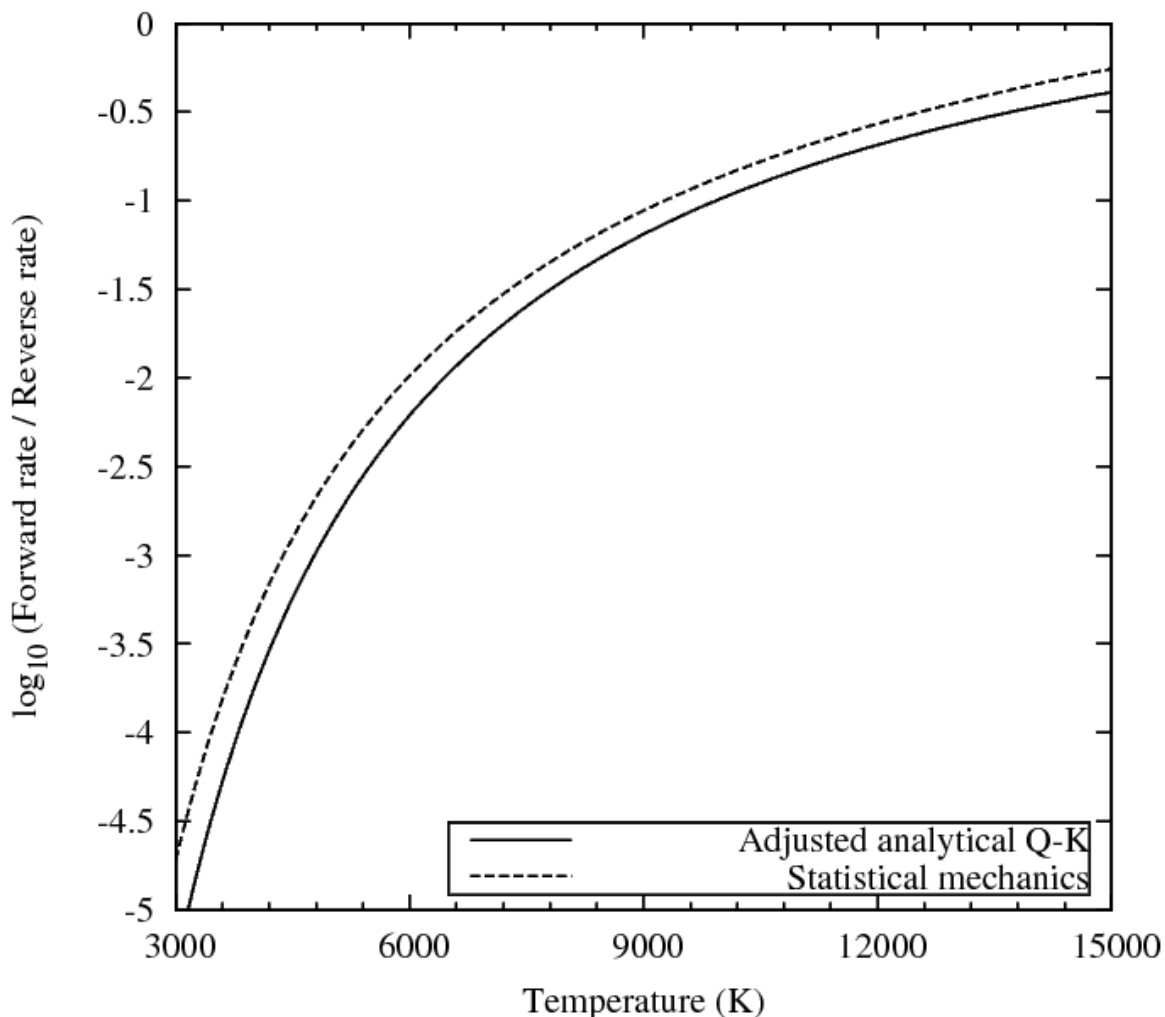
Figure 10 *The forward to reverse rate ratio for* $N_2 + O \leftrightarrow NO + N$.
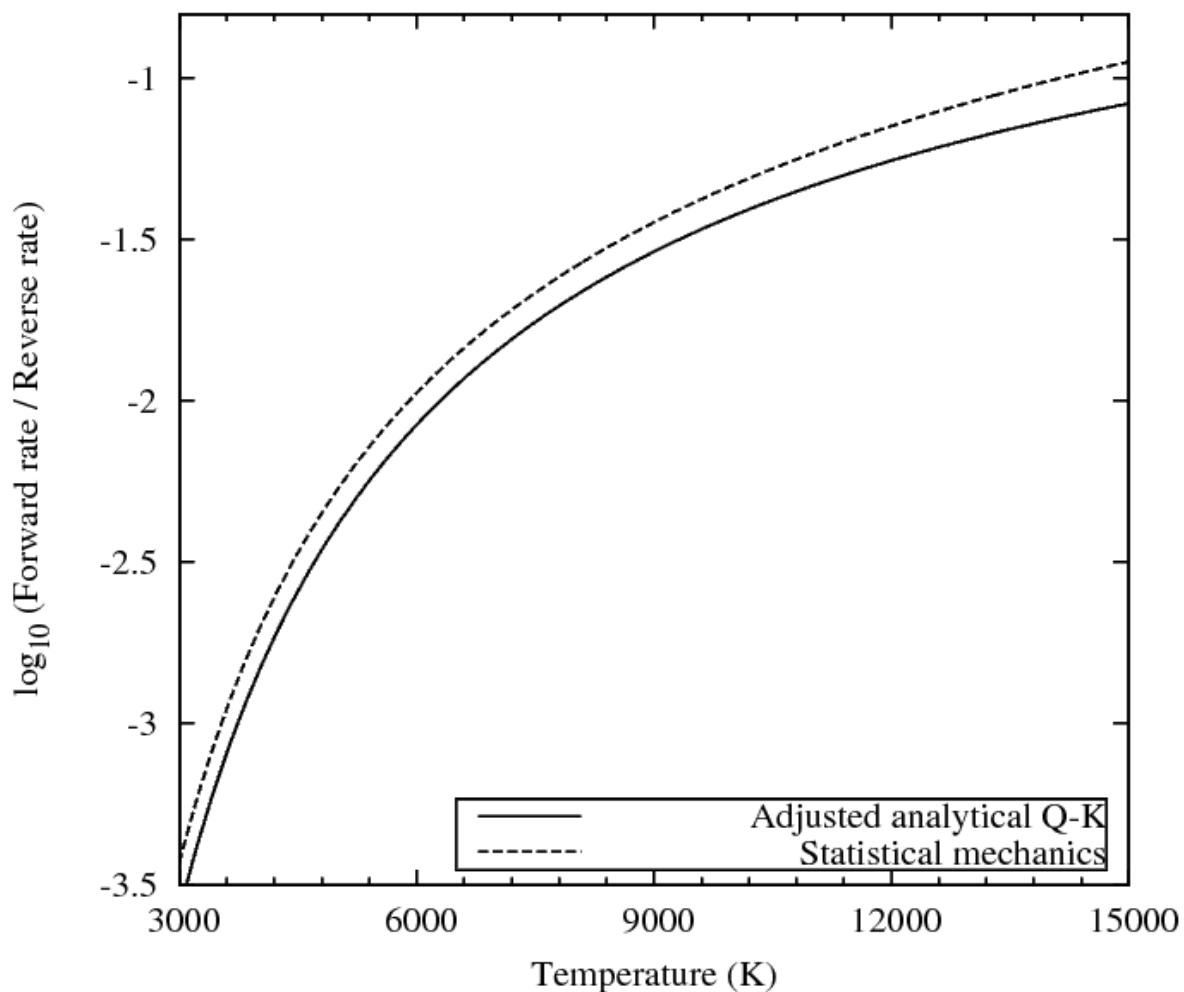
Figure 11 *The forward to reverse rate ratio for* $NO+O \leftrightarrow O_2+N$.

2.4.1 *Equilibrium exchange reactions*

Adiabatic box simulations are performed to measure the equilibrium rate coefficients for each of the four exchange reactions shown in Table 2. The cases have set up parameters identical to those for the equilibrium dissociation reactions presented in Section 2.3.2, and a 50% split of each species by number is used as the initial conditions.

Figure 12 shows the equilibrium reaction rate for the forward endothermic exchange reaction $NO+O \rightarrow O_2+N$. The TCE rate from Ref. [18], the DSMC data from
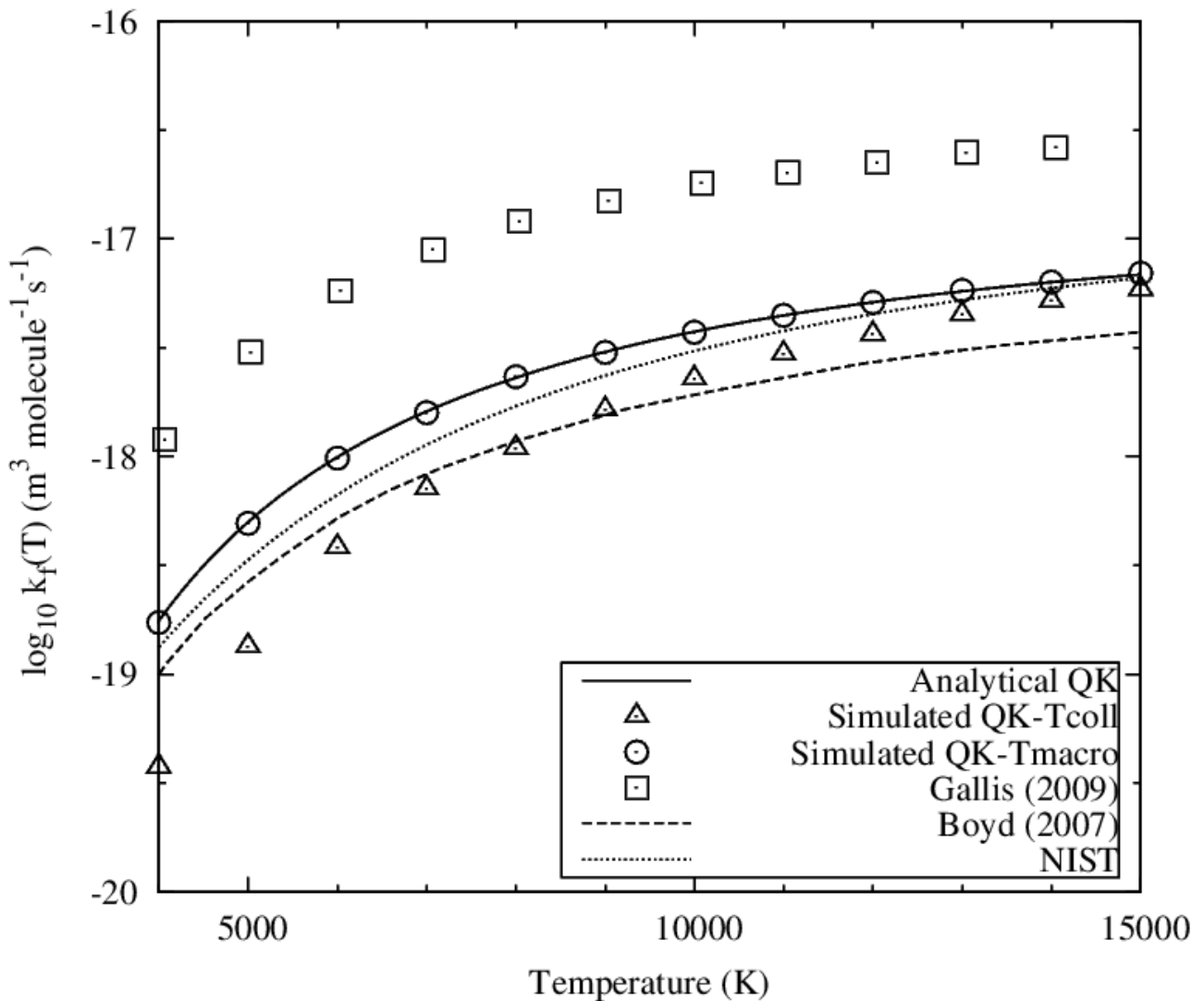
Figure 12 *Forward endothermic equilibrium exchange rate coefficient for* $NO+O \rightarrow O_2+N.$

Gallis *et al.* [2], and a rate representative of the National Institute of Standards and Technology (NIST) database [23] are also included. In addition to these, the *dsmcFoam* implementation for exchange has been calculated using two different definitions for temperature in Equations (34) and (35), these being the macroscopic and the collision temperature. The collision temperature has been used for all

dsmcFoam calculations in this paper and its definition is [1]:

$$T_{coll} = \left(m_r^{A,B} c_r^2 / (2k) \right) / \left(5/2 - \omega^{A,B} \right). \tag{37}$$

In his 2011 paper Bird [1] recommends that if the collision temperature is to be used then the exchange factor *a* in Equations (34) and (35) needs to be replaced by:

$$a' = \left[\left(5/2 - \omega^{A,B} \right)^b \Gamma\left(5/2 - \omega^{A,B} \right) / \Gamma\left(5/2 - \omega^{A,B} + b \right) \right] a \tag{38}$$

This step was considered necessary due to the inequality of macroscopic and collision temperatures when the parameter *b* is not equal to zero or unity. However, our *dsmcFoam* calculations for exchange showed no apparent difference whether T_{coll} was used in tandem with Equation (38) or not. It is desirable that the collision temperature be used in DSMC procedures rather than the macroscopic value as information should be passed upwards from the molecular level. However, it is clear from all our figures for exchange reactions that the use of macroscopic temperature in our *dsmcFoam* implementation produces equilibrium rates that match the Q-K analytical values. Such a result helps verify our coding, however the application of the collision temperature for exchange does produce results which are highly sensitive to the choice of the exponent parameter *b* in Equations (34) and (35). Averaging over all collisions $\bar{T}_{coll} = \bar{T}_{macro}$, however, $\bar{T}_{coll}^b \neq \bar{T}_{macro}^b$ unless *b* = 1 or 0 (note, the over bar represents average quantities). This can explain why there is closer agreement between the exchange rates found using T_{coll} and T_{macro} in Figures 13 and 14, as they use small values of the exponent *b* whereas there is an increased disparity between the T_{coll} and T_{macro} rates in Figures 12 and 15 as a larger value of *b* is employed.

The simulated Q-K rates using T_{coll} are seen in Figure 12 to fall within the range covered by the TCE and the NIST rates for temperatures in excess of around 7000 K.

It is interesting to note that the Gallis *et al.* [2] data, based on a DSMC implementation which did not consider the adjustment of activation energies, shows consistently higher reaction rates across the range of temperatures considered.

The corresponding reverse exothermic equilibrium rate for the $O_2 + N \rightarrow NO + O$ exchange reaction is shown in Figure 13. Additional experimental data from Gupta *et*
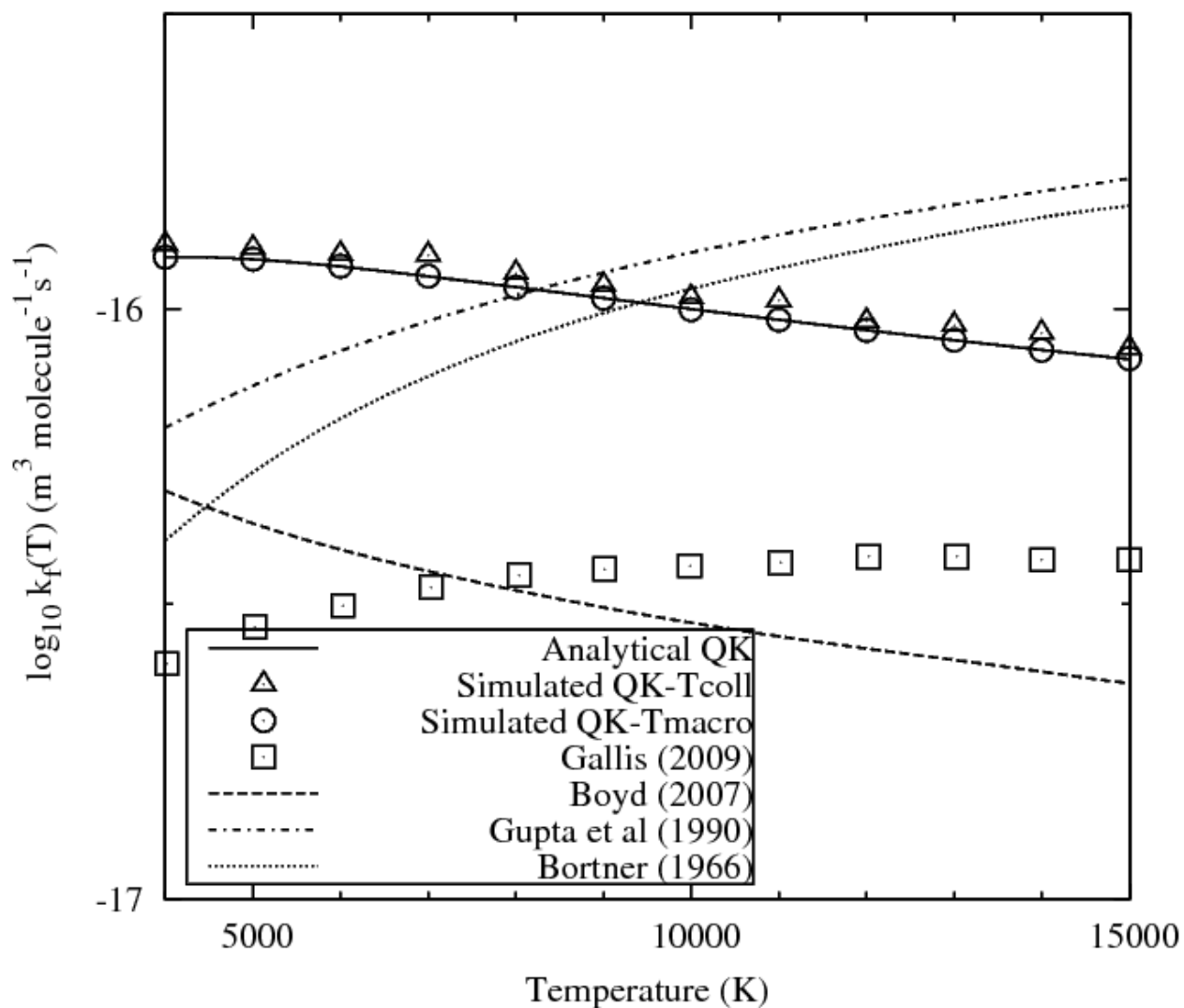
Figure 13 *Reverse exothermic equilibrium exchange rate coefficient for*

$$O_2 + N \rightarrow NO + O.$$

al. [24] and Bortner [25] have been included. Close agreement is observed between

the Q-K rates predicted by the collision and macroscopic temperatures because the coefficient *b* is small (0.1) for this reaction. The trend of decreasing reaction rate with temperature is similar for both Q-K and TCE, however the Q-K rates are higher across the range of temperatures studied and are closer of the results of Gupta *et al.* and Bortner. In comparison with the activation energy-adjusted Q-K approach presented in this paper, the previous incarnation of Q-K considered by Gallis *et al.* predicts lower rates for this reaction with their results being closer to the TCE rates.

Figure 14 depicts the forward equilibrium rate for the $N_2 + O \rightarrow NO + N$ reaction.
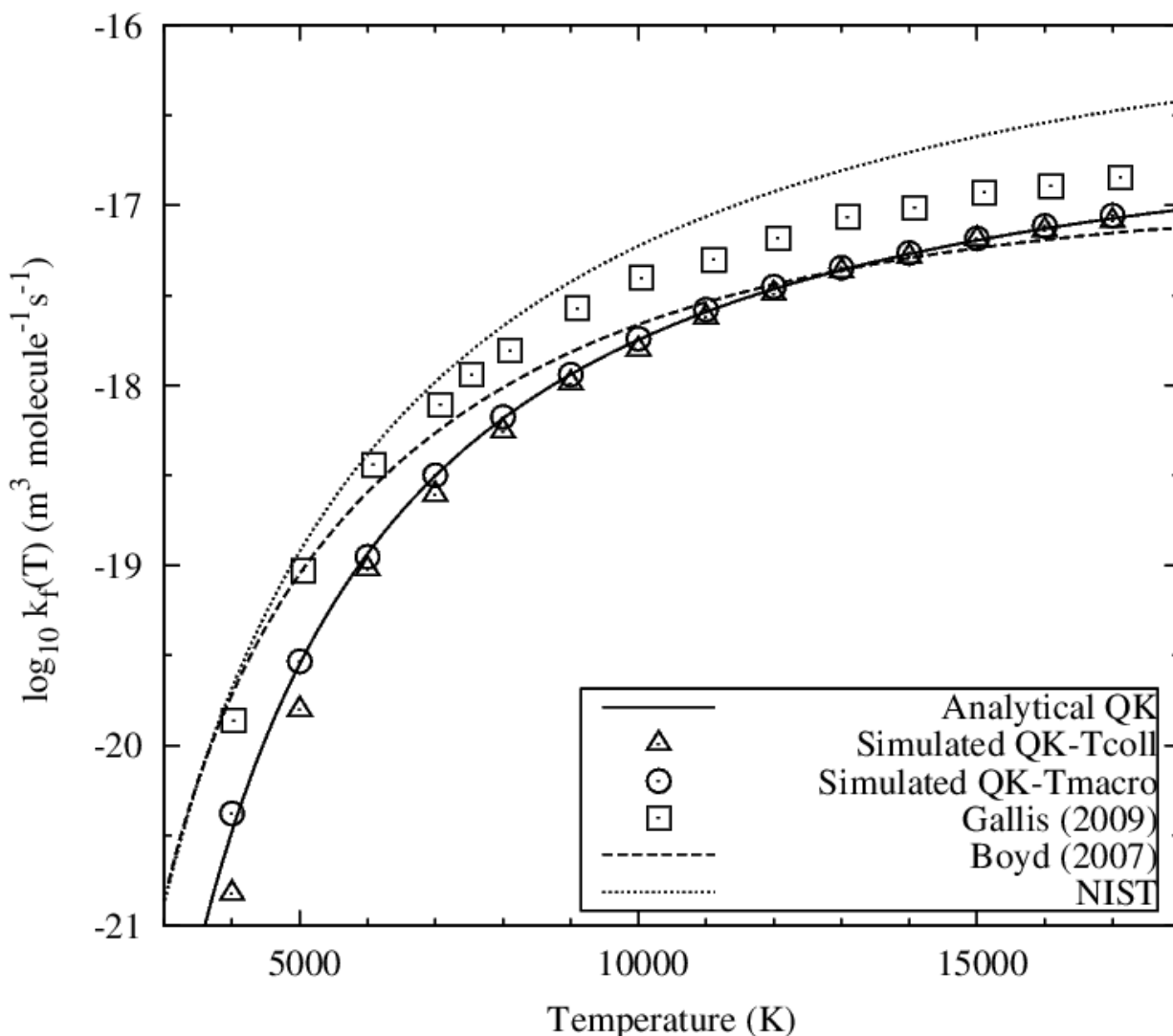
Figure 14 *Forward endothermic equilibrium exchange rate coefficient for*

$N_2 + O \rightarrow NO + N.$

Closer agreement is evident between the macroscopic and collision temperature based rates because *b* is small (0.15) for this reaction. In comparison with the TCE approach, the Q-K values agree closely at higher temperatures, while the DSMC calculations of Gallis *et al.* approach the TCE values at lower temperatures. The NIST rates are consistently higher than all of the DSMC approaches across the range of temperatures investigated.

The final equilibrium exchange case we consider is the reverse reaction
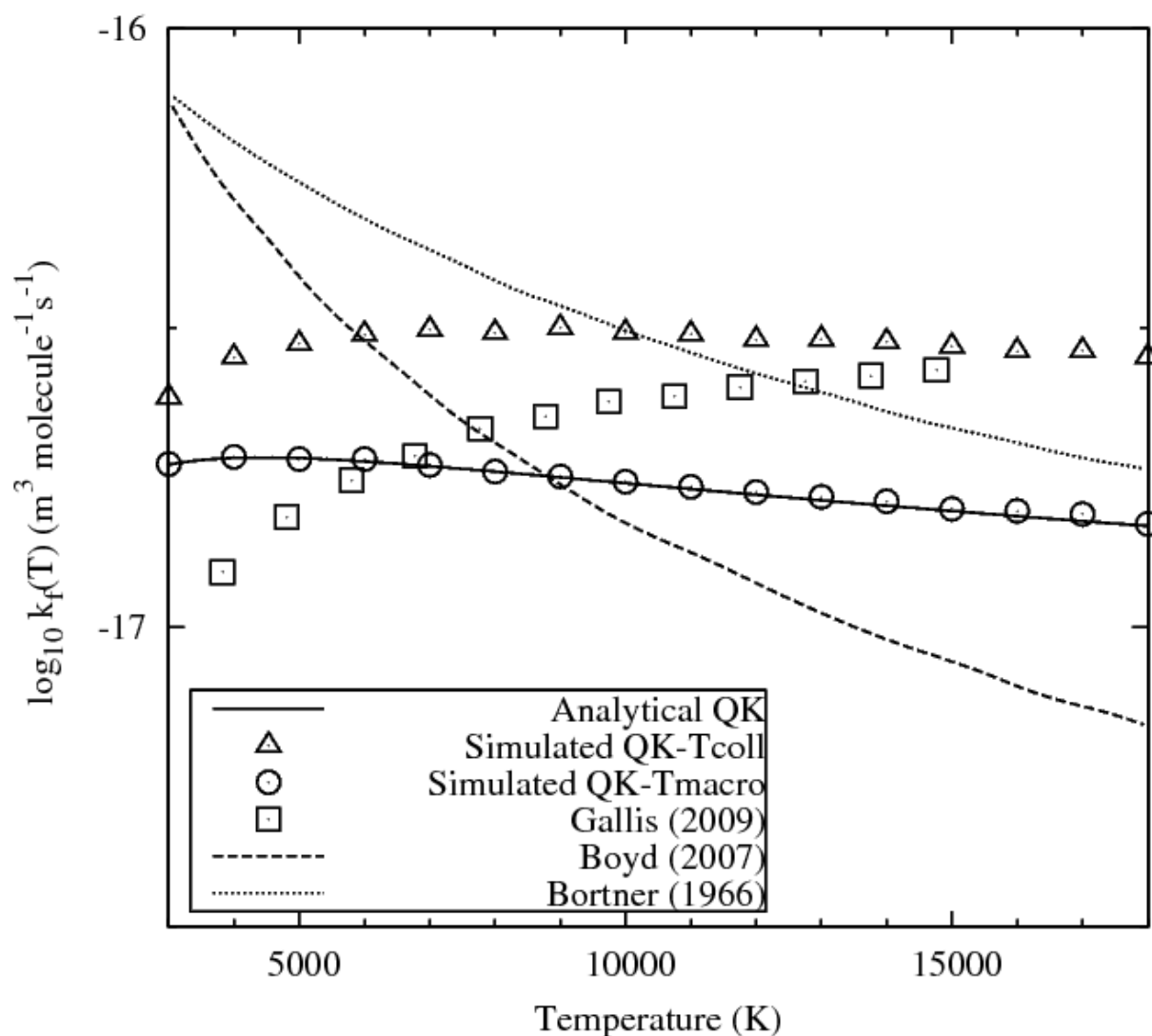
Figure 15 *Reverse exothermic equilibrium exchange rate coefficient for*
$NO+N \rightarrow N_2+O.$

$NO+N \rightarrow N_2+O$ and the reaction rates are plotted in Figure 15. The Q-K rates are a closer match to those of Boyd and Bortner in the lower temperature range, while the results of Gallis *et al.* more closely correlate with the TCE values in the middle temperature ranges. The Q-K predictions from *dsmcFoam* and those from Gallis *et al.* tend towards similar values above around 15,000 K, while the TCE rates are consistently below the Q-K values above approximately 8000 K. Although a similar trend is observed, the Q-K rates predicted using T_{coll} are consistently higher than those resolved using the macroscopic temperature because a higher value of *b* is employed (0.8) in Equation (35).

2.4.2 *Non-equilibrium exchange reactions*

Particle splitting and the subsequent non-equilibrium reaction process for exchange chemistry are considered in this section. The geometry, boundary, initial conditions, DSMC parameters and time-step size are identical to those described in section 2.3.3. An equal percentage of reactant species is employed at the start of the reaction.
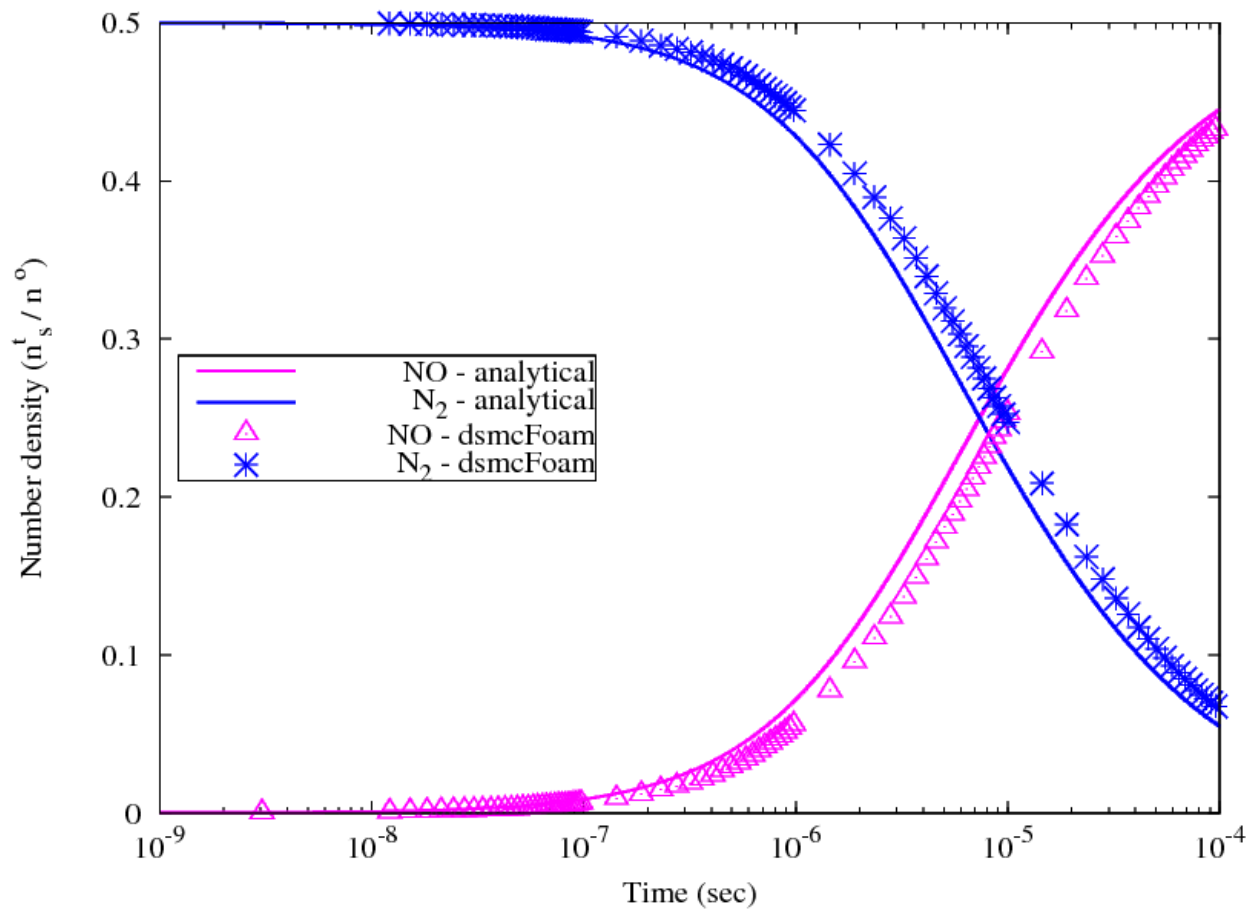
Figure 16 *Species concentrations during the forward exchange reaction* $N_2 + O \rightarrow NO + N$ *from an initial temperature of 20,000 K and pressure of 0.063 atm.*
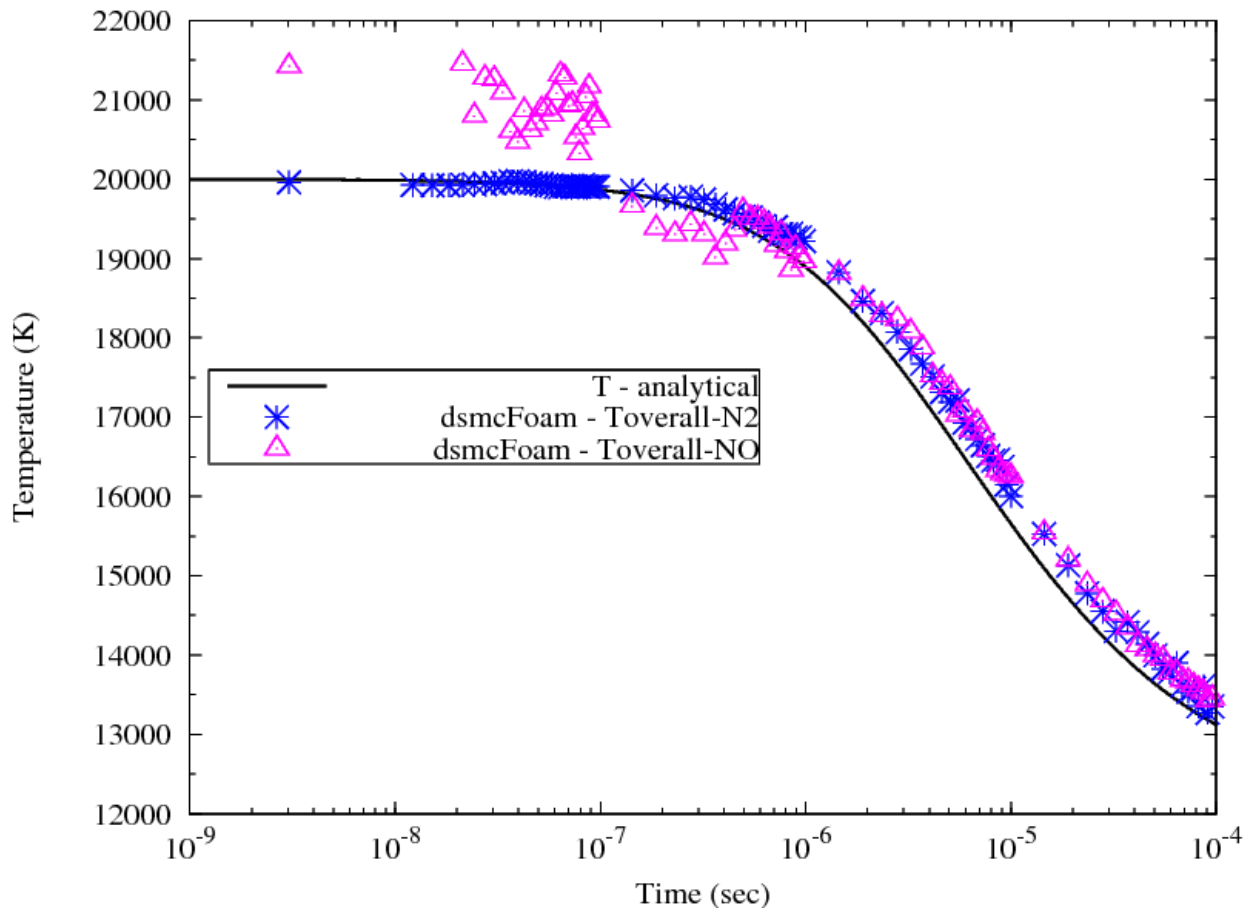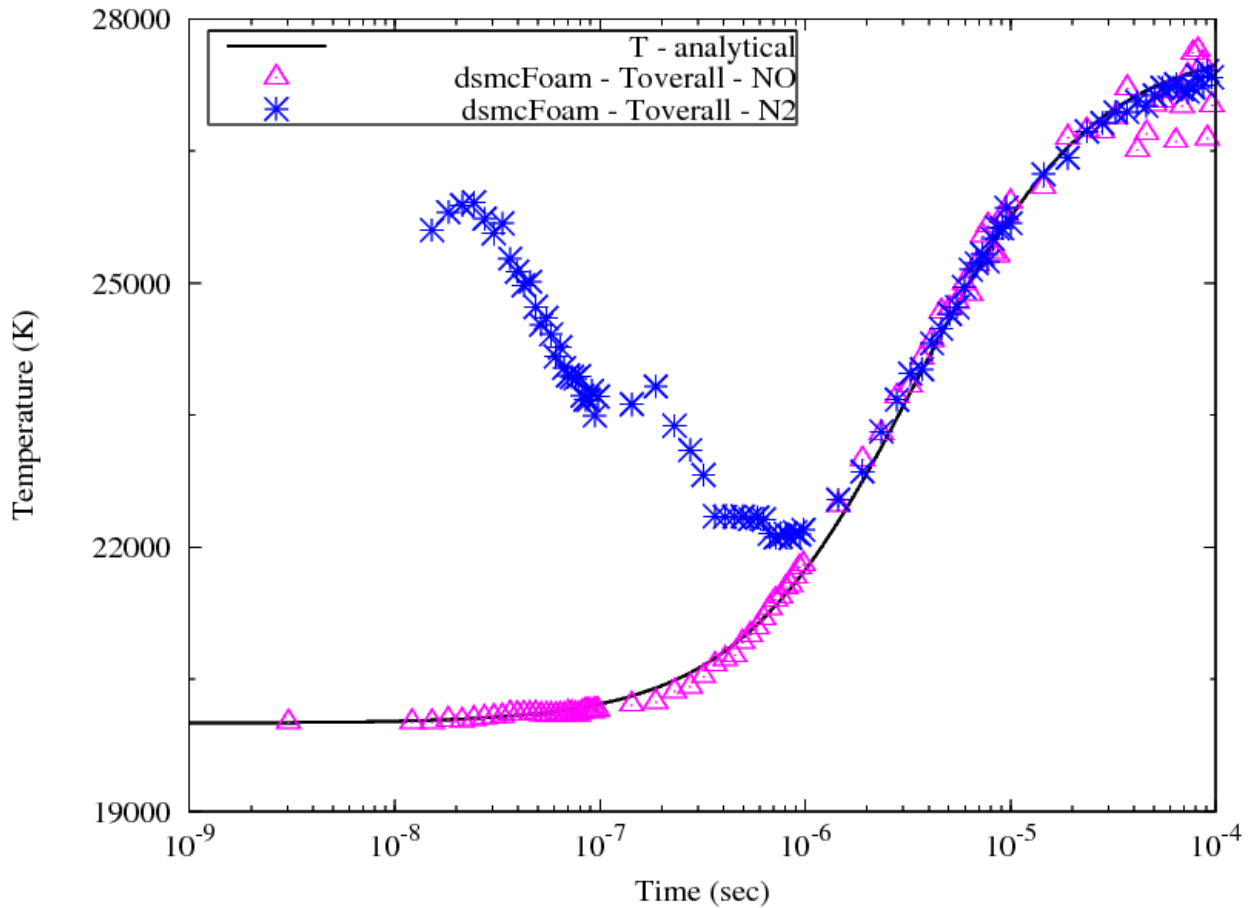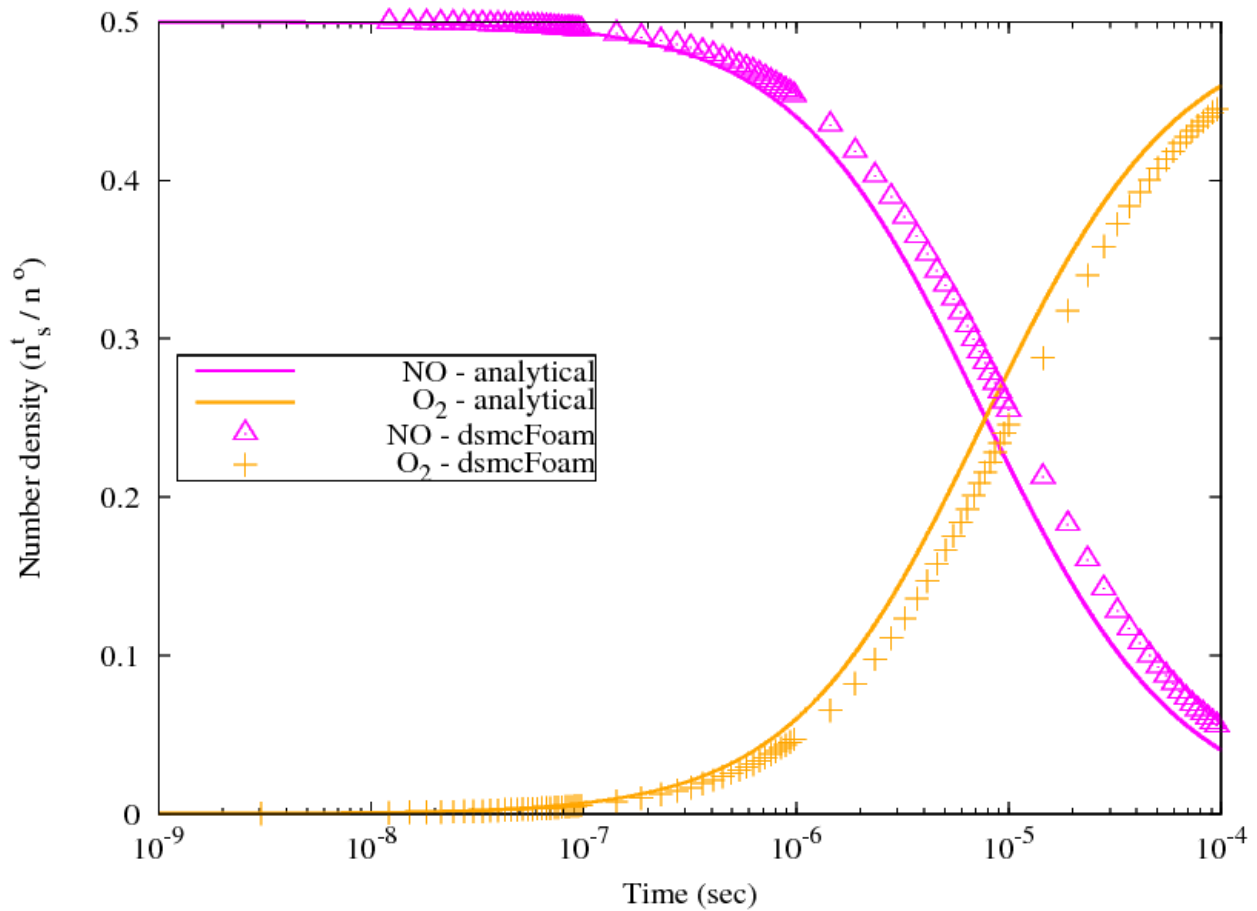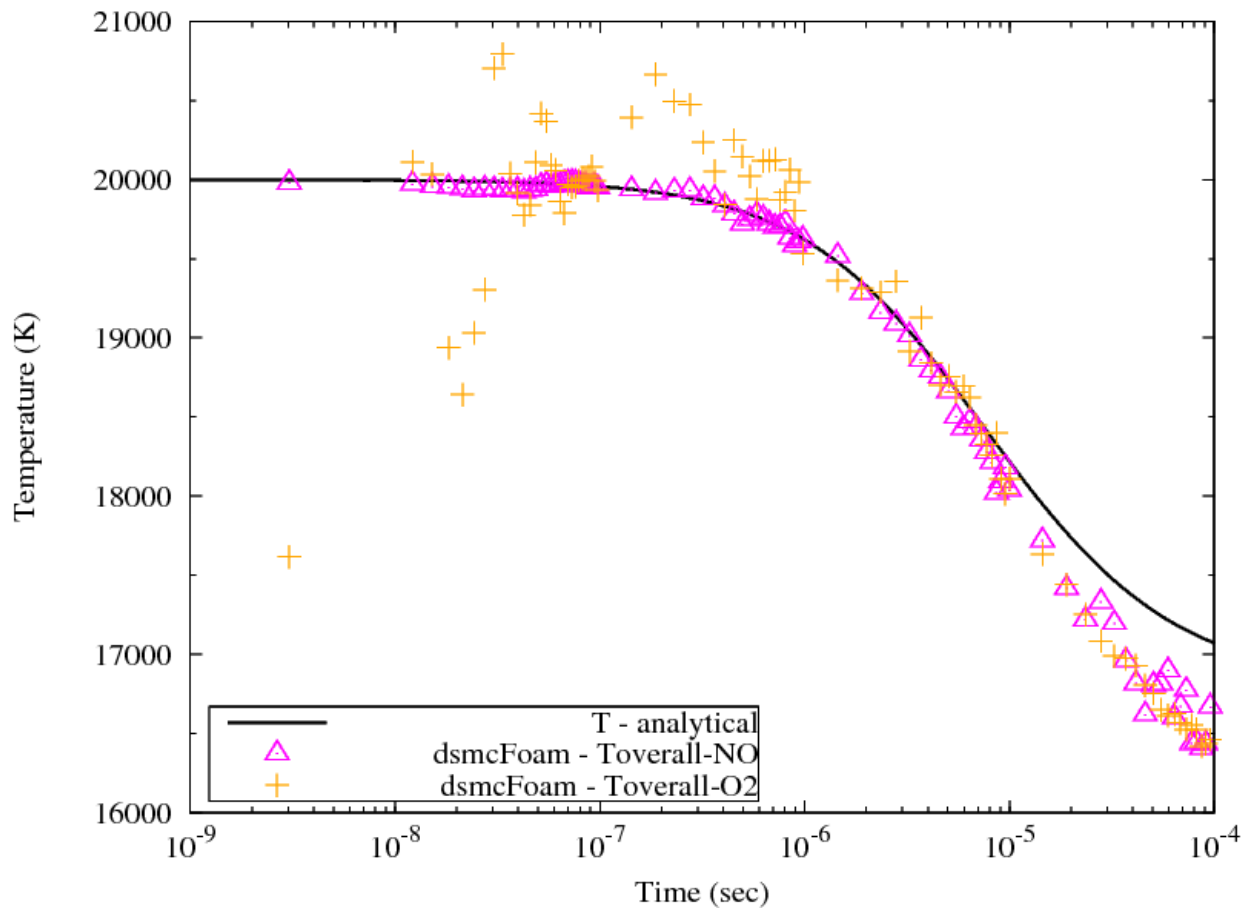
Figure 17 *Overall temperature for the forward exchange reaction*
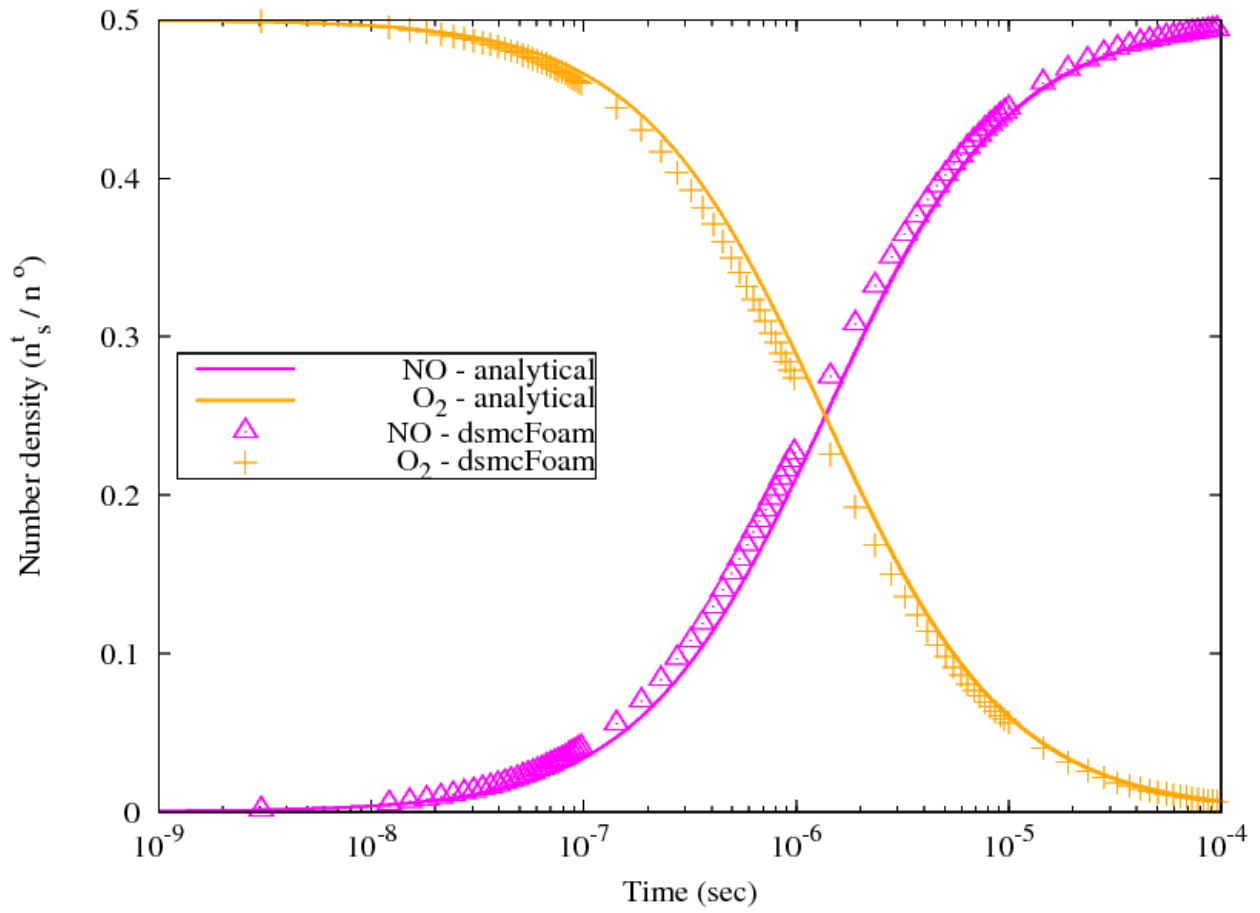$N_2 + O \rightarrow NO + N$ *from an initial temperature of 20,000 K and pressure of 0.063 atm.*

Figure 16 depicts the molar concentrations during the forward exchange reaction $N_2 + O \rightarrow NO + N$. Broad agreement between the analytical solution of Equation (27) and the Q-K results is observed. For the temperature field in Figure 17, the endothermic reaction shows a temperature decay from 20,000 K to approximately 13,200 K after 1×10^{-4} s has elapsed. Initial disequilibrium is highlighted by the differences in the overall temperatures as the nascent *NO* molecules begin to appear. The discord between the temperatures for the reactant molecule N_2 and the product molecule *NO* diminishes as the reaction proceeds towards equilibrium. In general, there is a satisfactory concurrence between the analytical Equation (27) and

dsmcFoam Q-K solutions.

Figures 18 and 19 show the molar concentration and temperature fields respectively for the exothermic reverse exchange reaction $NO + N \rightarrow N_2 + O$. Once again, very reasonable agreement is obtained between the analytical Equation (27) and the *dsmcFoam* Q-K predictions. The overall temperature field is seen to achieve equilibrium after a time of approximately 1×10^{-5} s, with a temperature of around 27,700 K being reached after 1×10^{-4} s. The *NO* overall temperature scatter, evident towards the end of the reaction, may be put down to statistical fluctuations as the *NO* becomes rapidly depleted.
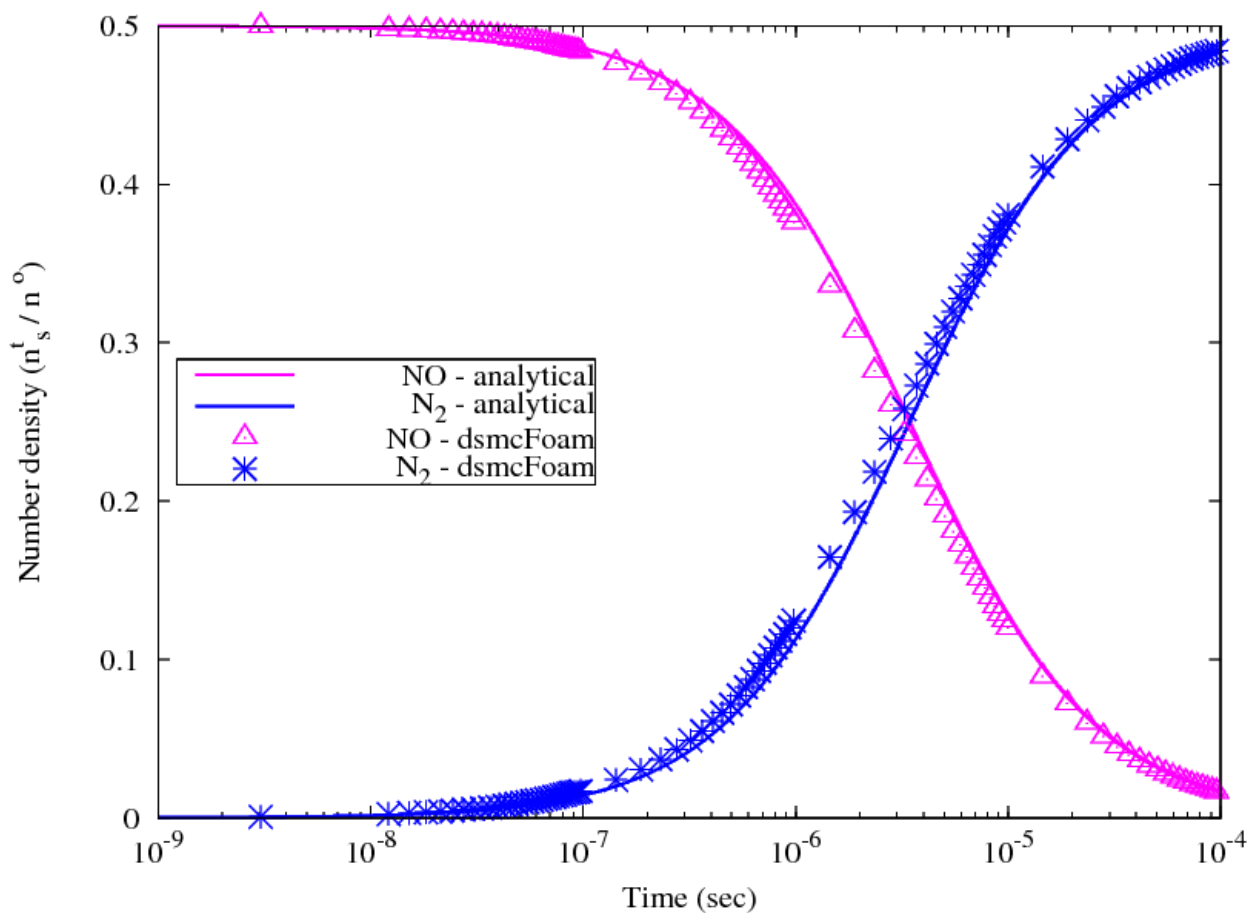
Figure 18 *Species concentrations during the reverse exchange reaction $NO + N \rightarrow N_2 + O$ from an initial temperature of 20,000 K and pressure of 0.063 atm.*
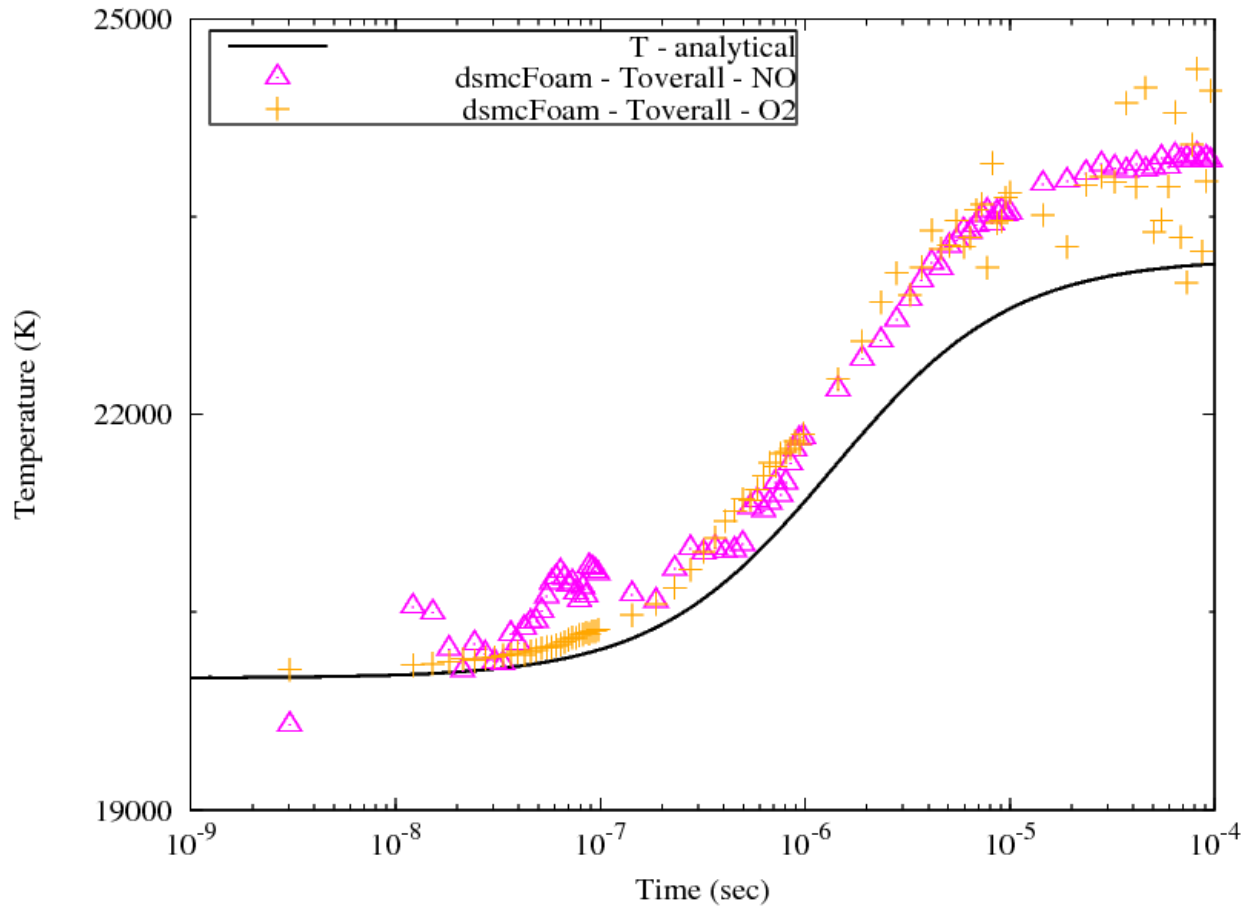
Figure 19 *Overall temperature for the reverse exchange reaction*

$NO+N \rightarrow N_2+O$ *from an initial temperature of 20,000 K and pressure of 0.063 atm.*

The results for the forward exchange reaction $NO+O \rightarrow O_2+N$ are shown in Figures 20 and 21. The molar concentrations are in reasonable agreement with the analytical values, however, the overall temperature for the Q-K prediction finishes approximately 500 K below the analytical one. It has been found that the Q-K solutions are particularly sensitive to the choice of the equilibrium coefficients *a* and *b* in Table 2 and this may have a bearing on the outcome for this particular reaction.

Finally, for the exchange reactions, Figures 22 and 23 demonstrate the results for the reverse exothermic exchange reaction $O_2+N \rightarrow NO+O$. Excellent agreement for

the species concentrations is found between the analytical and DSMC results, while the temperature values are, in general, satisfactory but do conclude with a difference of around 600 K towards the end of the reaction. The scatter in temperature towards the end of the reaction is due to the paucity of O_2 molecules as depletion ensues.

Figure 20 *Species concentrations during the forward exchange reaction $NO+O \rightarrow O_2+N$ from an initial temperature of 20,000 K and pressure of 0.063 atm.*

Figure 21 *Overall temperature for the forward exchange reaction*
$NO + O \rightarrow O_2 + N$ from an initial temperature of 20,000 K and pressure of 0.063
atm.

Figure 22 *Species concentrations during the reverse exchange reaction*
$O_2+N \rightarrow NO+O$ *from an initial temperature of 20,000 K and pressure of 0.063*
atm.

Figure 23 *Overall temperature for the reverse exchange reaction* $O_2 + N \rightarrow NO + O$ *from an initial temperature of 20,000 K and pressure of 0.063 atm.*

2.5 *Air reactions*

The complete set of 19 reactions shown in Table 1 is now considered in an adiabatic box filled with air at 0.063 *atm* pressure at an initial composition of 79% N_2 and 21% O_2. Three cases are considered for initial temperatures of 30,000 K, 20,000 K and 10,000 K. Other simulation parameters are identical to those described in section 2.3.3.

Figures 24 to 29 show the evolution of species and overall temperature for the three initial temperatures considered. In general, the Q-K predictions of the constituent

evolution agree well with the analytical result although there is an under-prediction of *NO* towards the end of the reactions. Oxygen scatter towards the tail of the reaction is due to its rapid depletion as the reactions progress. Considering the overall temperature field for the gas mixture, very good agreement between the DSMC and analytical solutions is evident for each case, with any scatter being explained by the extinction of the O_2 and *NO* molecules towards the end of the reaction process.
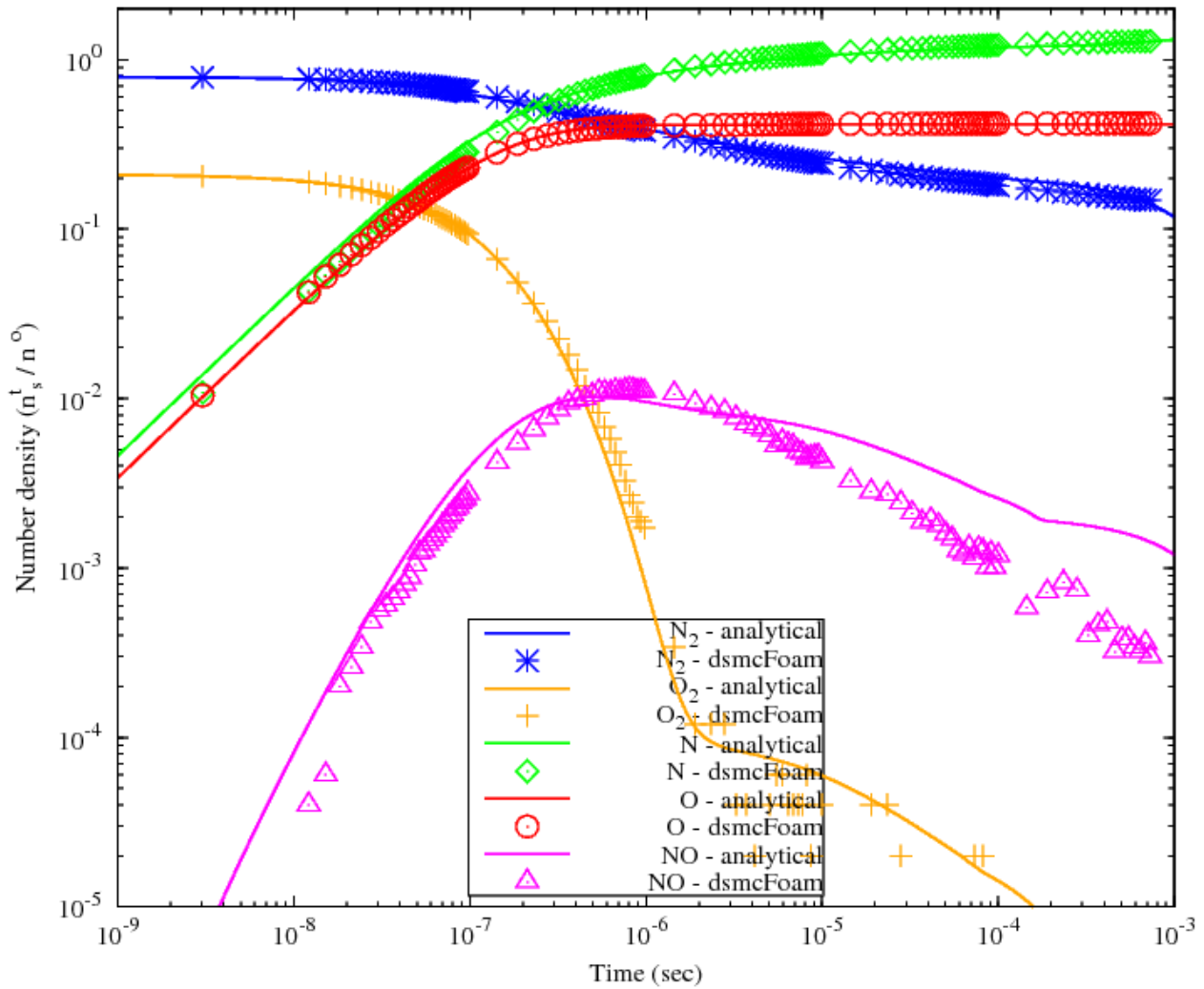
Figure 24 *Species concentrations during the decomposition of air from an initial temperature of 30,000 K and pressure of 0.063 atm.*
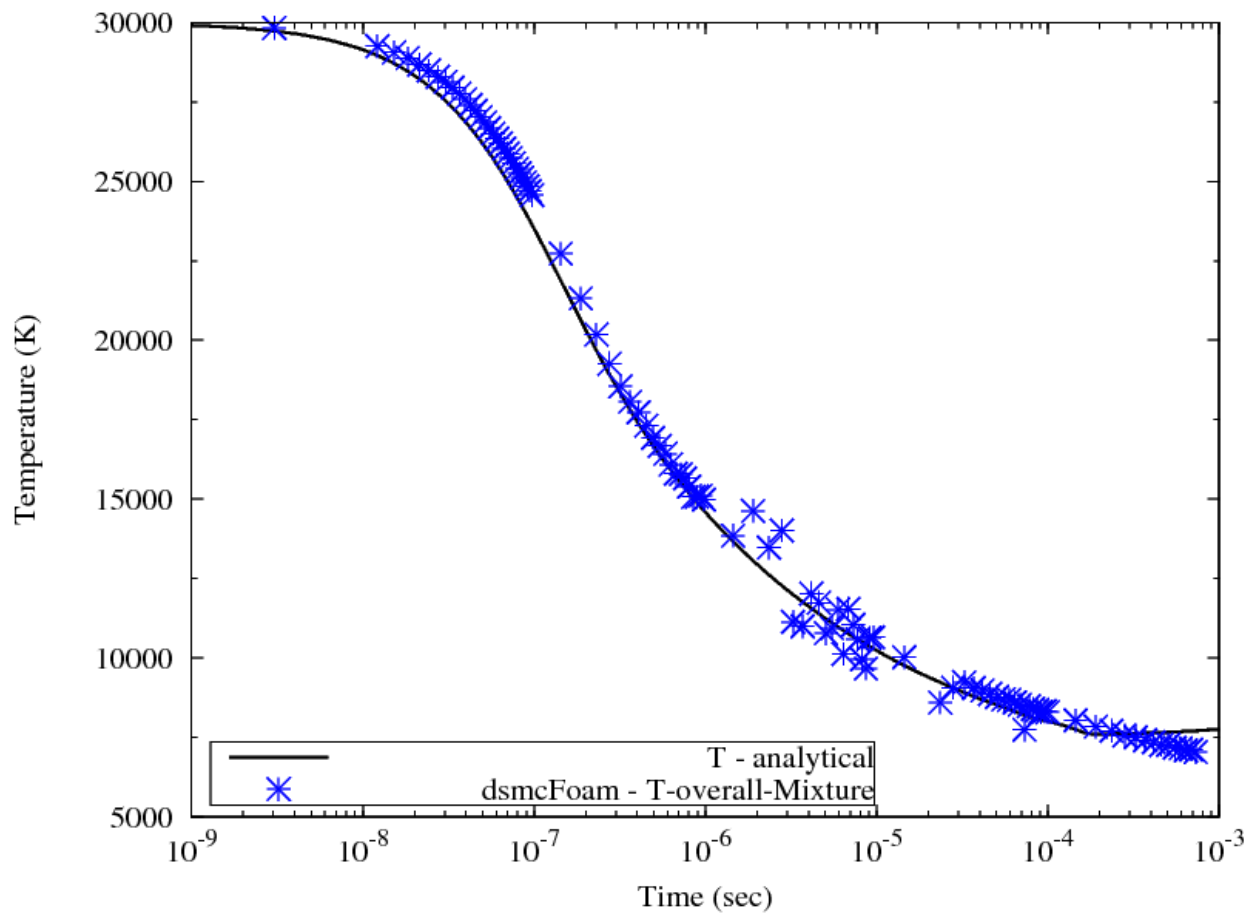
Figure 25 *Overall temperature evolution of the gas mixture during the decomposition of air from an initial temperature of 30,000 K and pressure of 0.063 atm.*
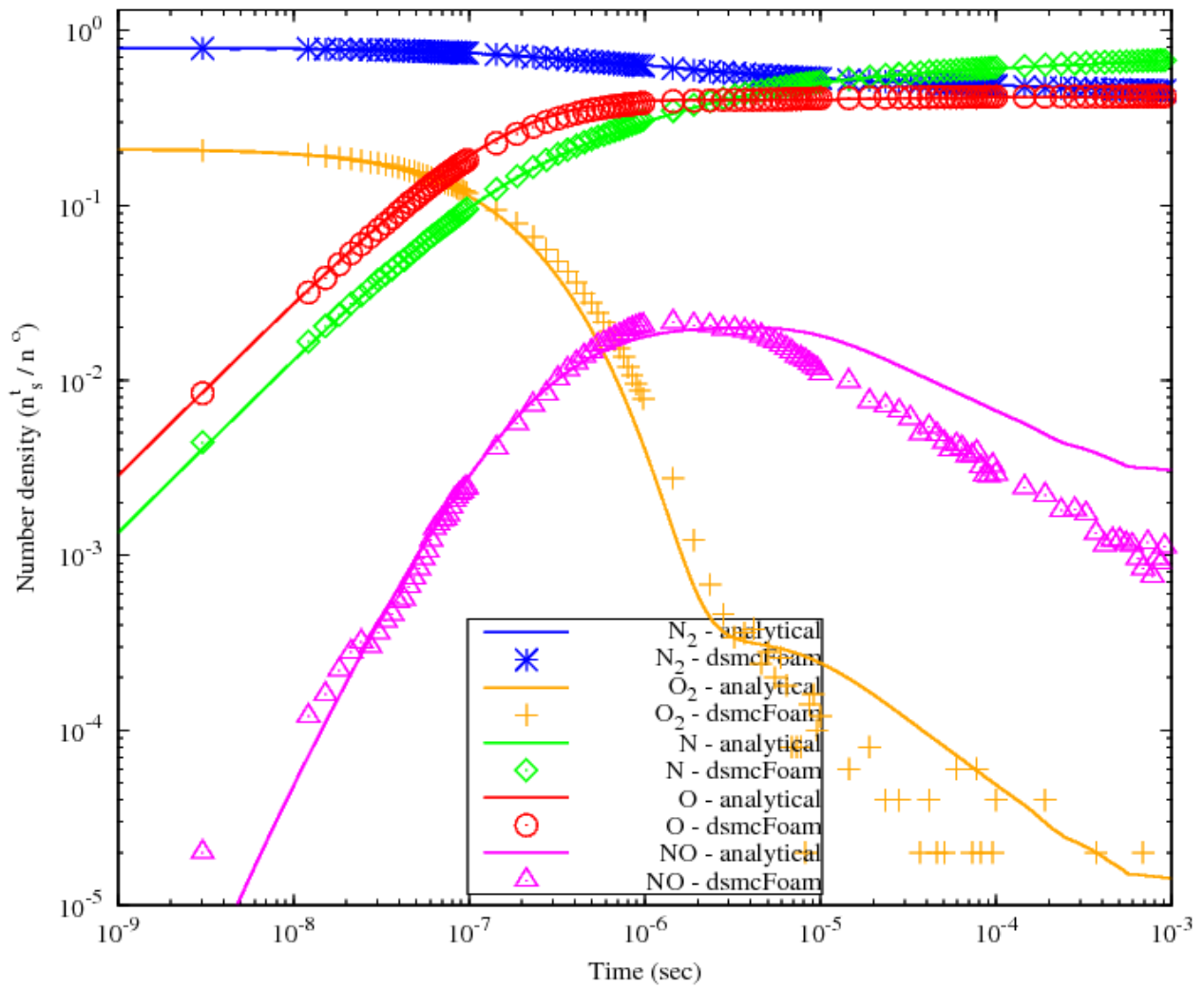
Figure 26 *Species concentrations during the decomposition of air from an initial temperature of 20,000 K and pressure of 0.063 atm.*
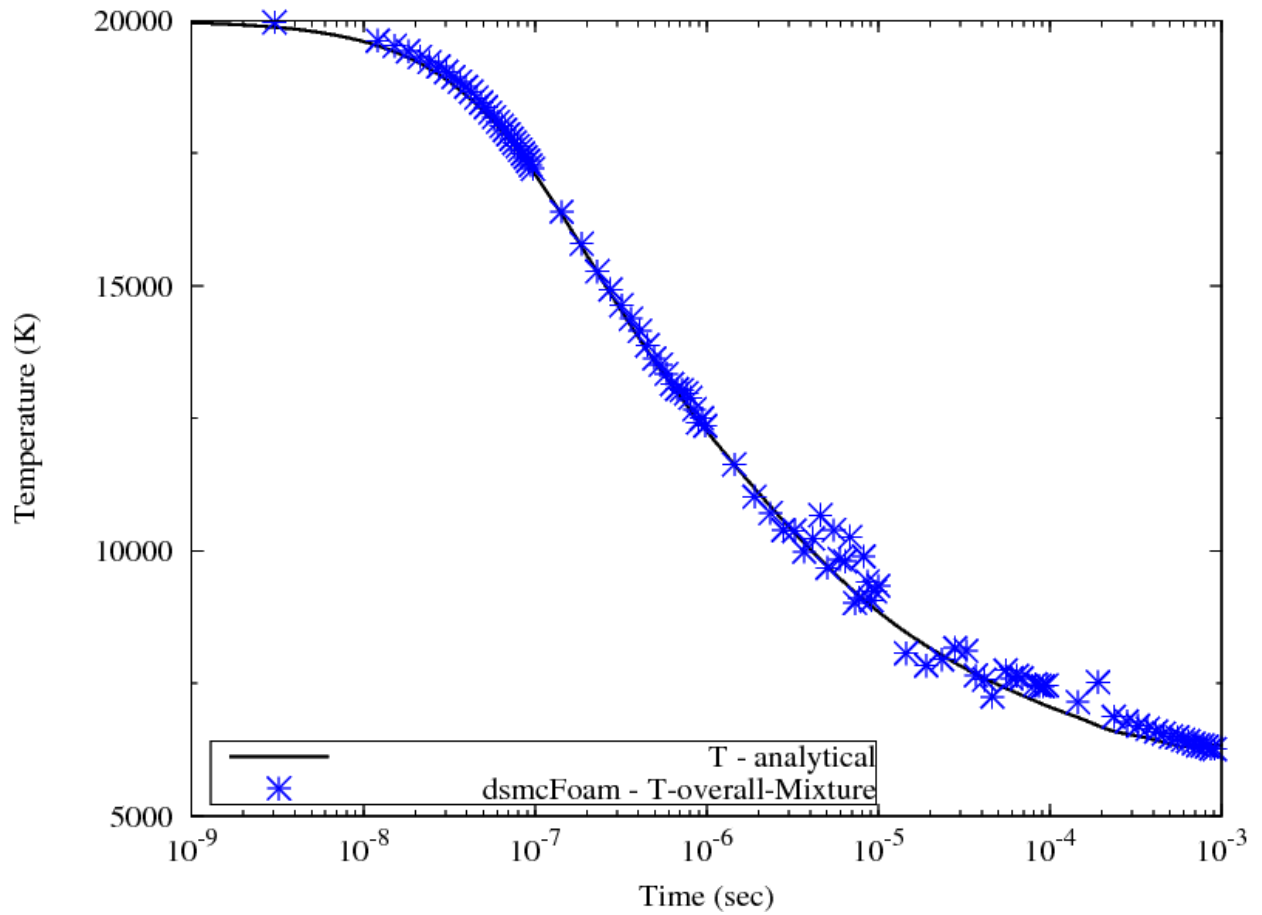
Figure 27 *Overall temperature evolution of the gas mixture during the decomposition of air from an initial temperature of 20,000 K and pressure of 0.063 atm.*
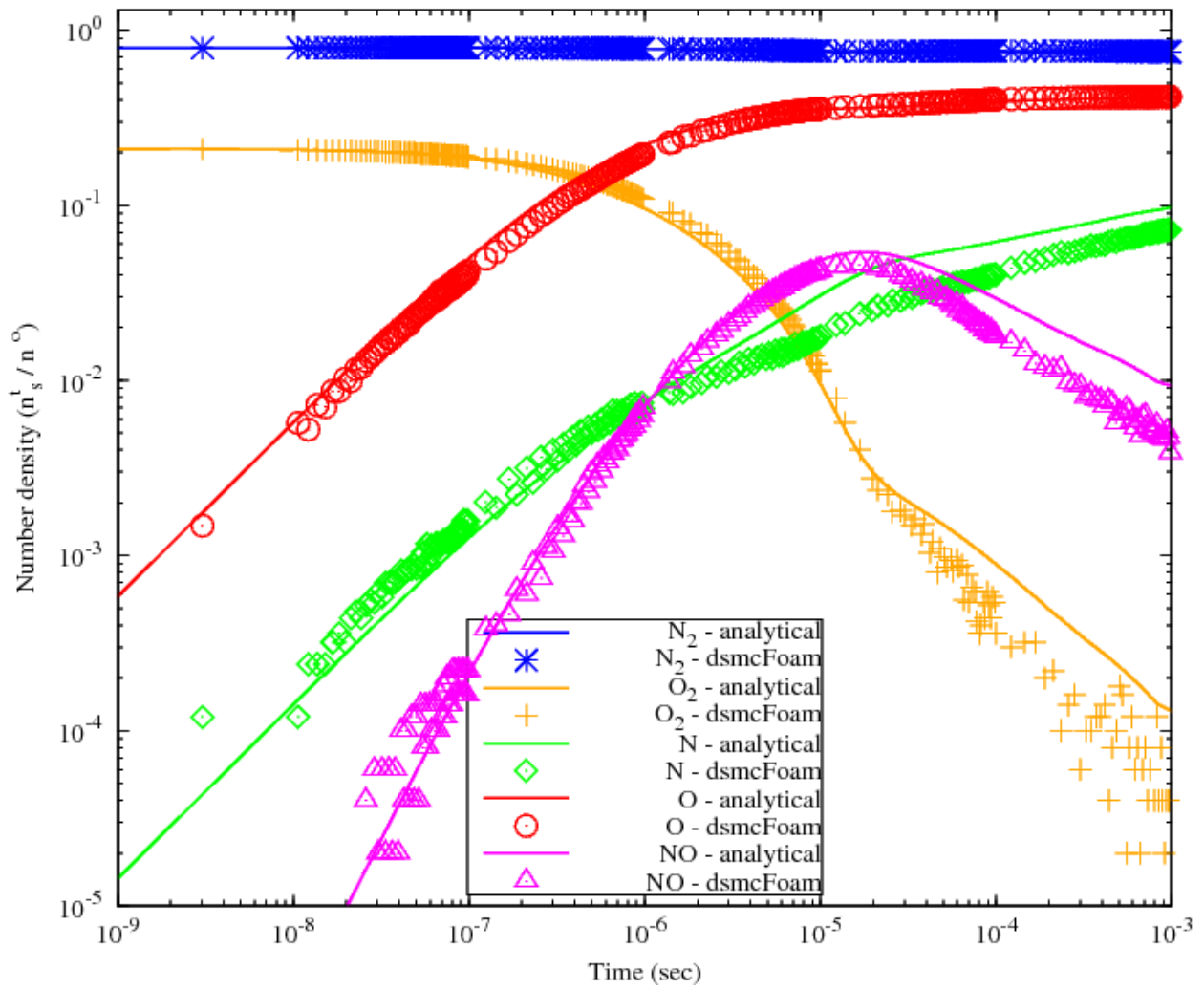
Figure 28 *Species concentrations during the decomposition of air from an initial temperature of 10,000 K and pressure of 0.063 atm.*
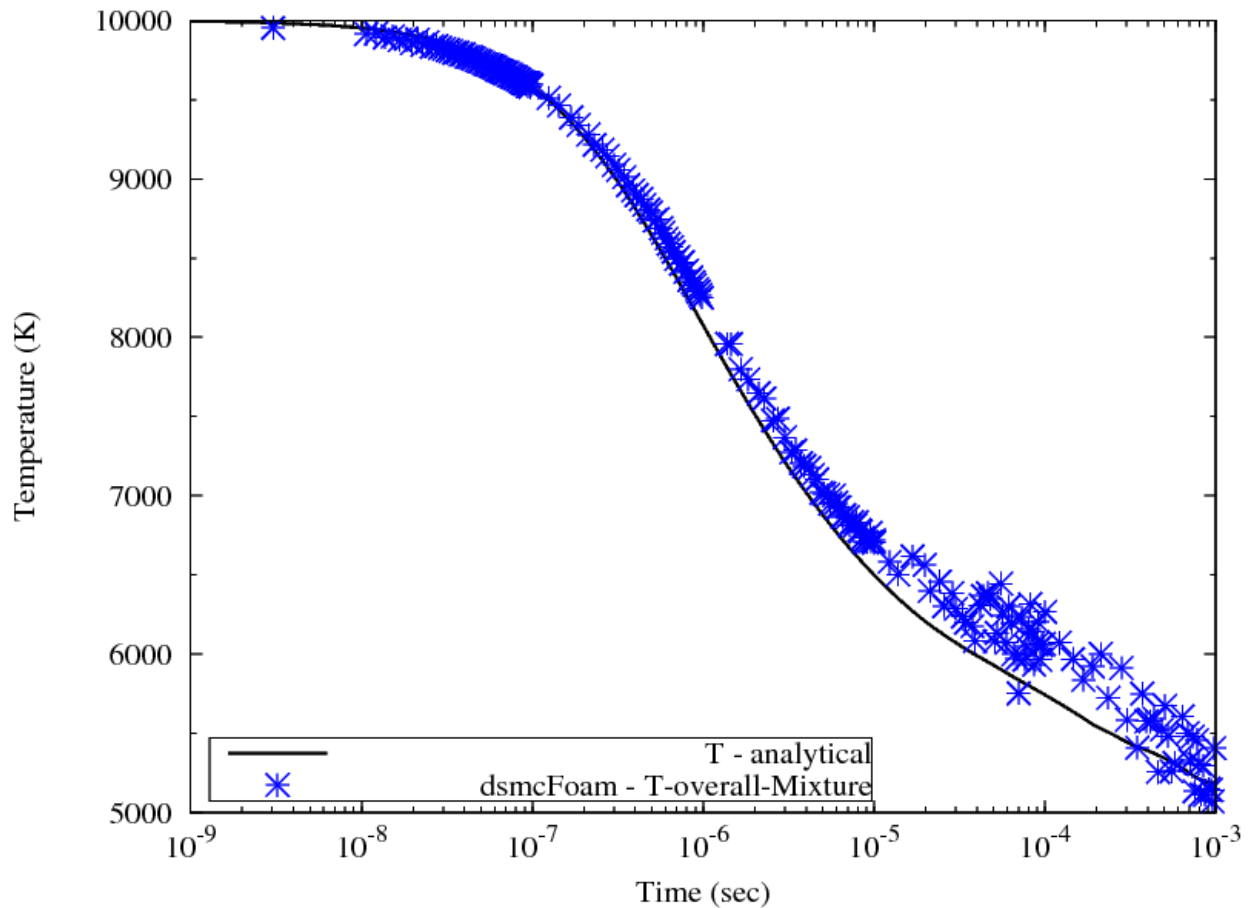
Figure 29 *Overall temperature evolution of the gas mixture during the decomposition of air from an initial temperature of 10,000 K and pressure of 0.063 atm.*

3.0 A hypersonic flow case

In order to test the *dsmcFoam* implementation of the Q-K chemistry model in a real scenario a hypersonic flow test case is simulated. This consists of high speed, rarefied air flow over a 2D cylinder at the atmospheric free stream conditions shown in Table 3.

Table 3 *Free stream conditions for test case of hypersonic air cross flow over a 2D cylinder.*

Cylinder diameter	2 *m*
Flow velocity	6813 *m/s*
Free stream temperature	187 *K*
Cylinder wall temperature	1000 *K*
N_2 number density	1.13×10^{20} *m^{-3}*
O_2 number density	3.031×10^{19} *m^{-3}*

These conditions correspond to the Earth's atmosphere at 86 *km* altitude and a Mach number of 24.85. The cylinder walls are fully diffuse, and two cases are considered; one with no reactions, and one with all 19 chemical reactions shown in Table 1 activated. Comparisons are made with the equivalent solutions using the established DSMC code MONACO which employs TCE chemistry. In all cases the rotational and vibrational collision numbers are set to 5 and 50, respectively, and the TCE Arrhenius rates for dissociation and exchange are provided from the Q-K analytical equilibrium values, using Equation 9 for dissociation and Equations (32) and (33) for exchange. The mesh size for the *dsmcFoam* study is 240,000 cells with a time-step fixed at $1 \times 10^{-7} s$ and, following particle sensitivity trials, there were 23.4 million DSMC particles in the system at steady-state. For the MONACO study the domain contains 175,000 cells with automatic sub-cell generation and the total number of DSMC particles at steady-state is 37.5 million. In addition, cell-based, variable time-steps are used such that the ratio of the time step to mean collision time in each cell is approximately 0.2. We suggest that this test case be considered as a reference 2D benchmark trial for future DSMC chemistry implementations.

Figures 30 to 35 show the reacting and non-reacting comparisons between the DSMC codes for velocity, density and temperature, respectively, along the stagnation

streamline. For the non-reacting case it is clear from Figure 30 that the velocity profiles predicted by both codes along the stagnation streamline are in close agreement, and the shock region covers distance between approximately 26 and 40 *cm* from the cylinder stagnation point. The species density profiles for N_2 and O_2 are almost equivalent, as shown in Figure 32, while Figure 34 demonstrates that the peak translational, rotational and vibrational temperatures are in very close agreement.

With all 19 reactions activated, the velocity, density and temperature profiles along the stagnation streamline are again compared. As the chemical reactions that occur are mainly characterised by endothermicity, the local enthalpy is reduced and the maximum shock stand-off distance moves to a position closer to the vehicle (approximately 0.36 *m*) in comparison with the non-reacting case (0.4 *m*).

Figure 33 shows that the stagnation streamline densities for N_2 and *NO* calculated by each code are in relatively close agreement. Although the trends are similar, the values for the atomic species *N* and *O* predicted with *dsmcFoam* (Q-K) are in excess of those determined by MONACO (TCE). However, the opposite is true for O_2, with the MONACO (TCE) code producing values exceeding those of *dsmcFoam* (Q-K). The increased number of dissociation events when using Q-K may be qualitatively explained with reference to Wysong *et al.* [19]: the magnitude of the lower level vibrational cross-sections for the Q-K method would mean that more dissociation events are likely, compared with the TCE approach, in non-equilibrium flows with relatively low-vibrational excitation, such as high-altitude re-entry.

Significant reductions in the values of all three temperature modes under reacting flow conditions are evident in Figure 35, with both codes predicting a peak translational temperature along the stagnation streamline of approximately 20,000 *K*. This is in contrast to the non-reacting case, which has a peak translational magnitude of approximately 25,000 *K*. The peak values for rotational and vibrational

temperature are also in close agreement, however, the general *dsmcFoam* Q-K temperature values show a small but consistent shift to the left in comparison with the MONACO-based ones. This effect is consistent with the differences in the shock structure indicated by the left-ward velocity-shift shown in Figure 31.

Figures 36 and 37 show the contours of Mach number and *NO* density for each code, respectively. It is clear that the diffuse nature of the shock has been captured by both codes. Although differences exist between the results of the codes for the predicted velocity and temperature fields, it is evident that the local Mach numbers are in close agreement. For the *NO* field it is seen that small differences are evident between the solutions in this qualitative comparison, with the Q-K approach appearing to predict a thinner species layer in the range approaching the peak *NO* values. Nonetheless, the general flow features appear to be similar for both chemistry approaches.

The temperature modes are shown in Figures 38 to 40 and the fields of translational, rotational and vibrational temperatures show, in general, a similar qualitative concurrence in all areas of the flow field, with only subtle differences apparent in certain regions.

Finally, the surface properties are shown in Figures 41 to 48. The surface pressure values are in very close agreement between the codes, for both reacting and inert conditions as seen in Figures 41 and 42. A reduction of almost 100% for the heat flux on the cylinder is evident when comparing the reacting to the non-reacting case. It is clear that the process of dissociation has led to a reduced flow energy and a consequential reduction of energy transfer to the body. For reacting conditions, the peak-value of the heat flux is 64 kW/m^2 for TCE, and 67 kW/m^2 for Q-K. This difference of 4.6 % represents a similar margin to the range of peak-heat fluxes found in a separate case study of non-reacting flow over a 2D cylinder using a variety of DSMC codes [26]. Figures 45 to 48 show the surface temperature-jump and velocity-

slip predictions for inert and reacting conditions. The general trends are similar for both MONACO and *dsmcFoam*, however there appears to be a greater level of disparity at some locations on the cylinder surface compared with the results for pressure and heat-flux, with *dsmcFoam* predicting generally higher values of slip and jump.

3.   Conclusions

An open source DSMC chemistry model based on the Q-K approach has been developed for use in high-speed, rarefied gas flows. The code, called *dsmcFoam*, has been written within the framework of the open source CFD software suite OpenFOAM. Benchmark test cases demonstrate the successful implementation of the Q-K code into *dsmcFoam* and comparisons with analytical results for dissociation and exchange reactions showed a satisfactory degree of concurrence. Differences in the predicted equilibrium rates for Q-K exchange have been highlighted when macroscopic and collision temperatures are used. New air reaction rates for exchange have been determined, based on the Q-K approach, and presented in Arrhenius form. A test case was run for hypersonic cross flow over a 2D cylinder, and the *dsmcFoam* (Q-K) results were found to be in broad agreement with the established DSMC code MONACO which employs TCE procedures for its reaction modelling. Differences in predicted species profiles along the stagnation streamline for Q-K and TCE have been qualitatively explained. This hypersonic test case is suggested as a reference 2D benchmark trial for future DSMC chemistry implementations.
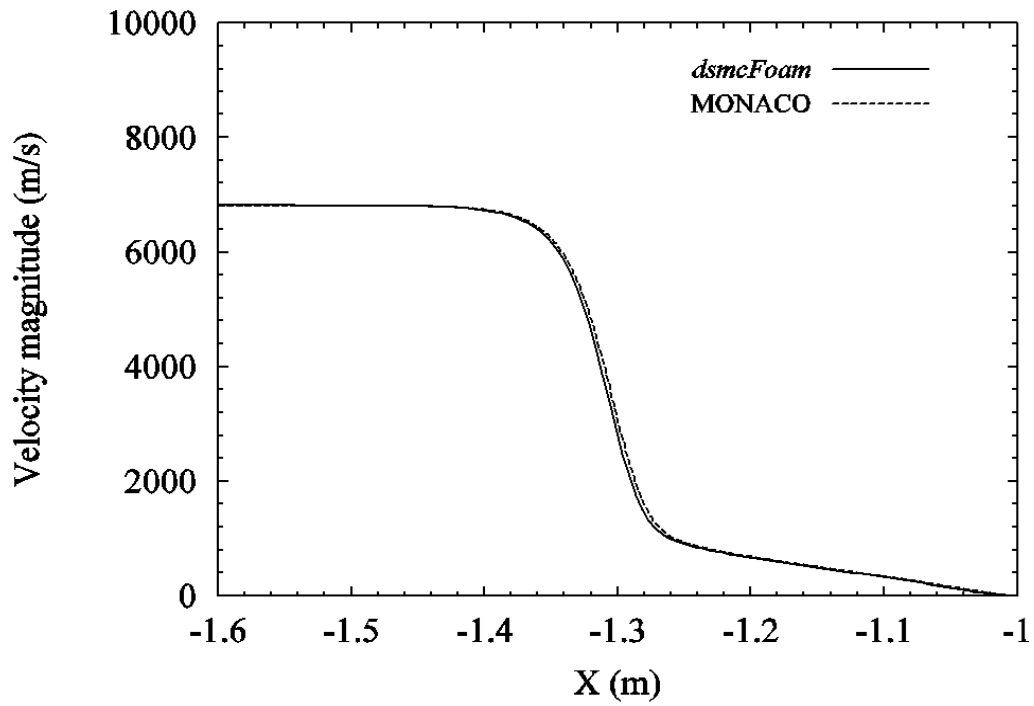
Figure 30 *Velocity profile along the stagnation streamline for non-reacting air flow over a 2D cylinder.*
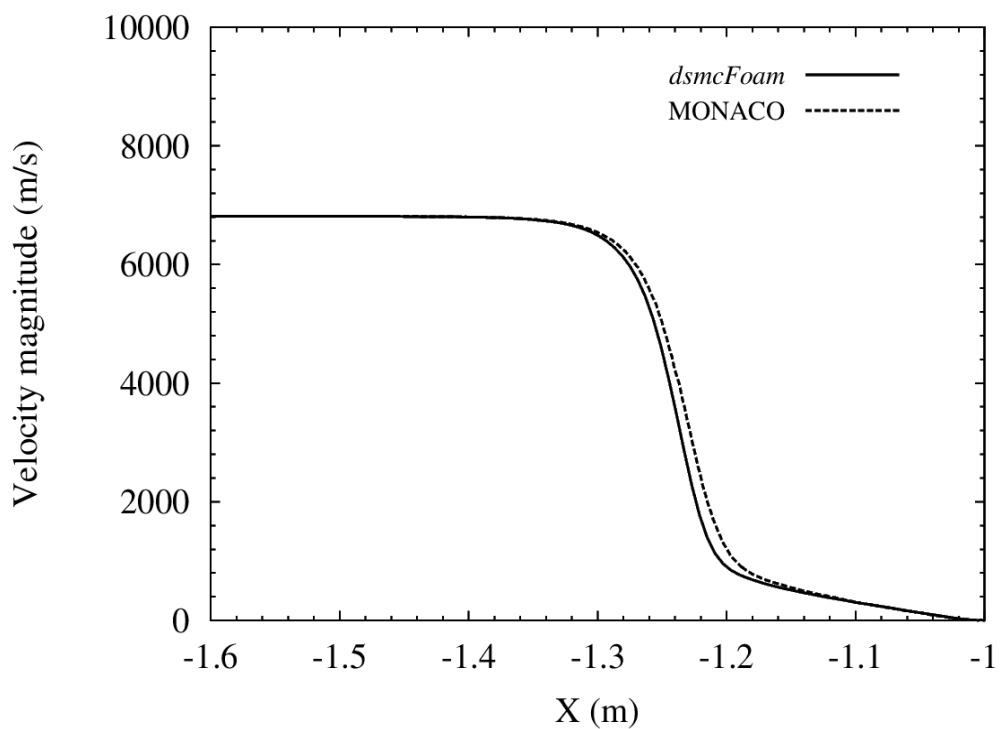
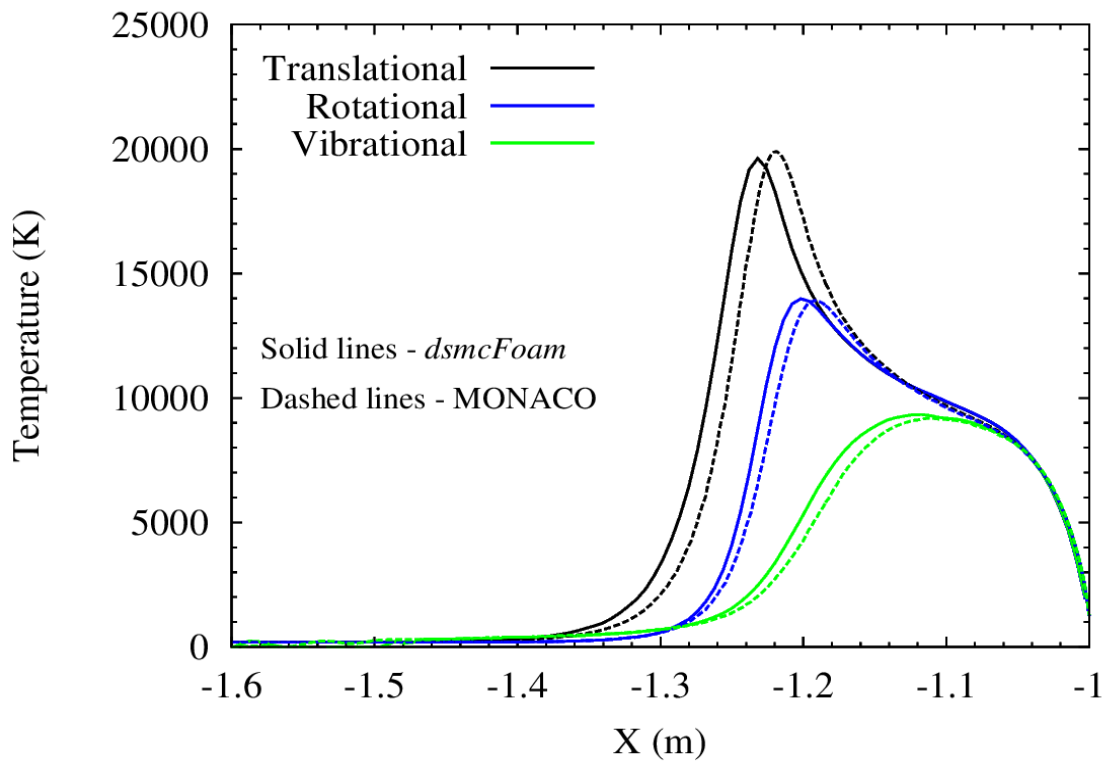**Figure 31** *Velocity profile along the stagnation streamline for reacting air flow over a 2D cylinder.*
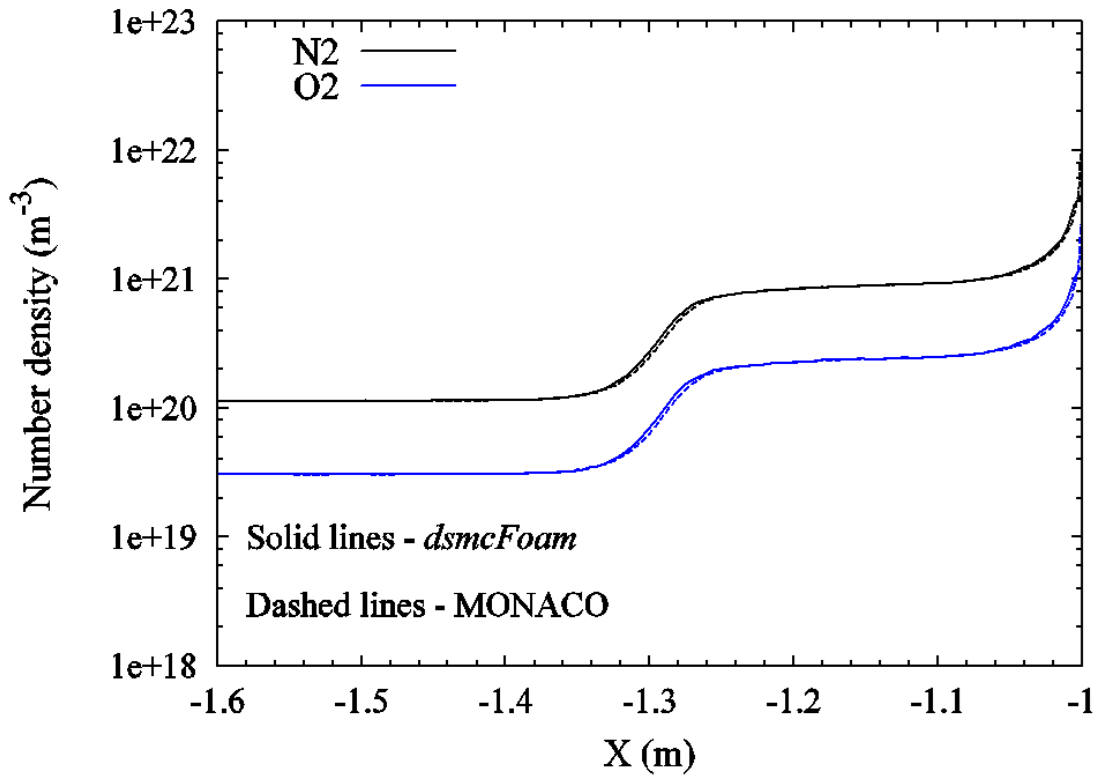
Figure 32 *Number density profile along the stagnation streamline for non-reacting air flow over a 2D cylinder.*
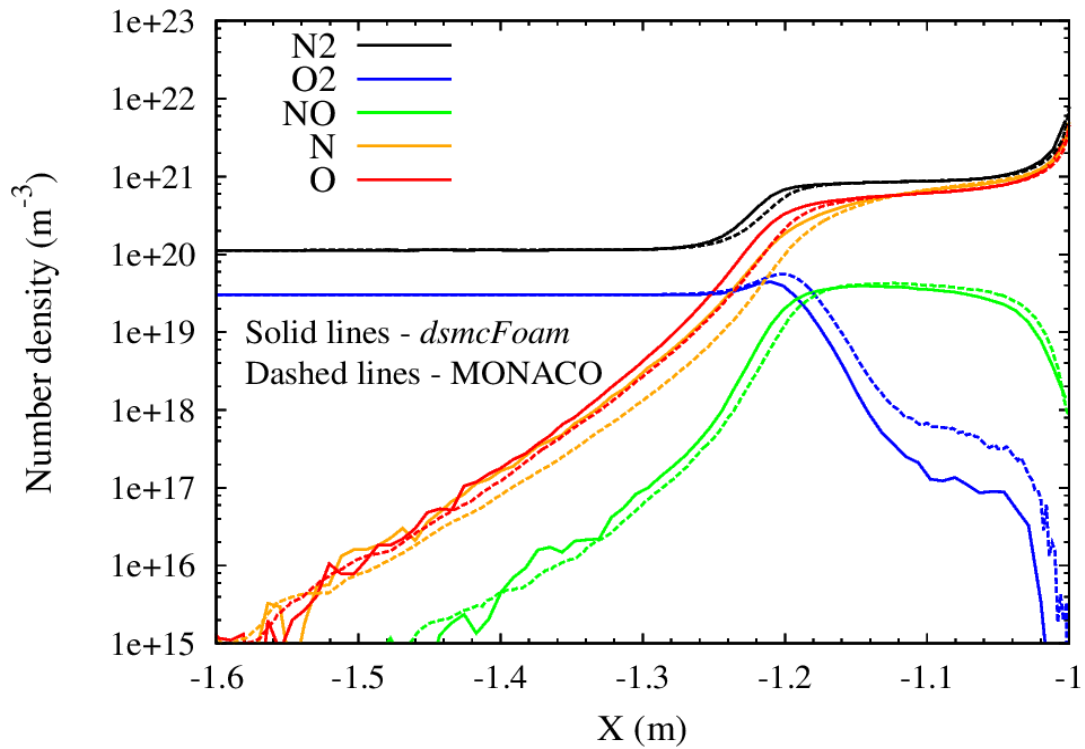
Figure 33 *Number density profile along the stagnation streamline for reacting air flow over a 2D cylinder.*
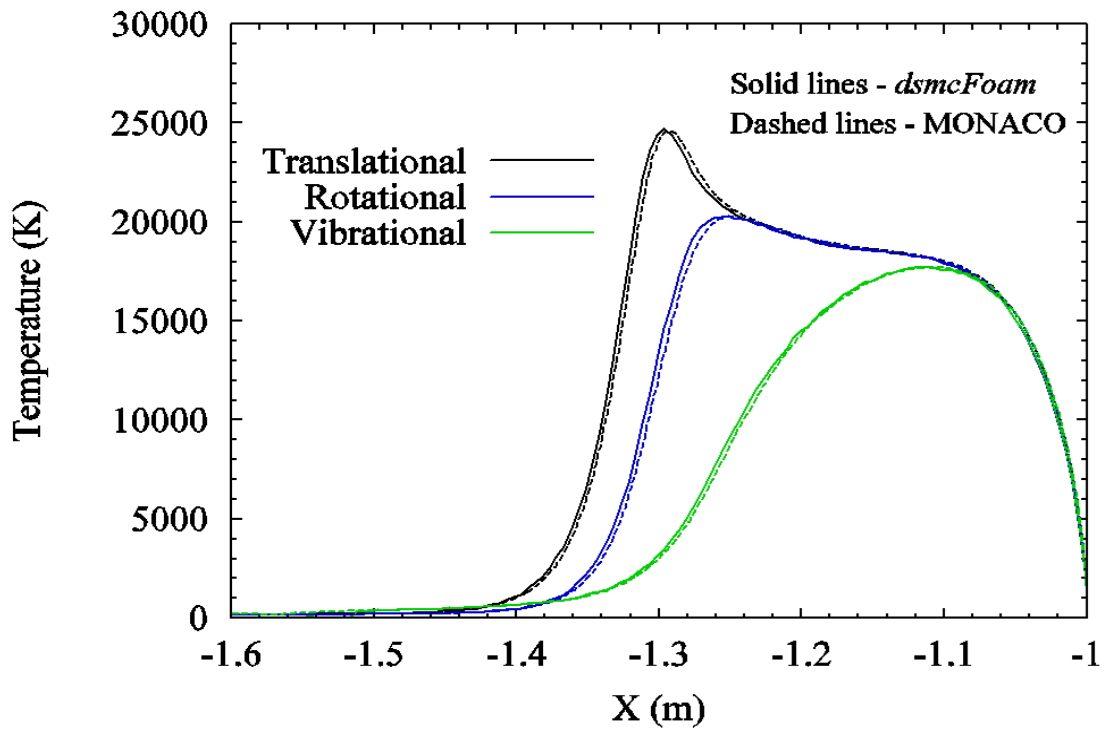
Figure 34 *Temperature profile along the stagnation streamline for non-reacting air flow over a 2D cylinder.*

Figure 35 *Temperature profile along the stagnation streamline for reacting air flow over a 2D cylinder.*
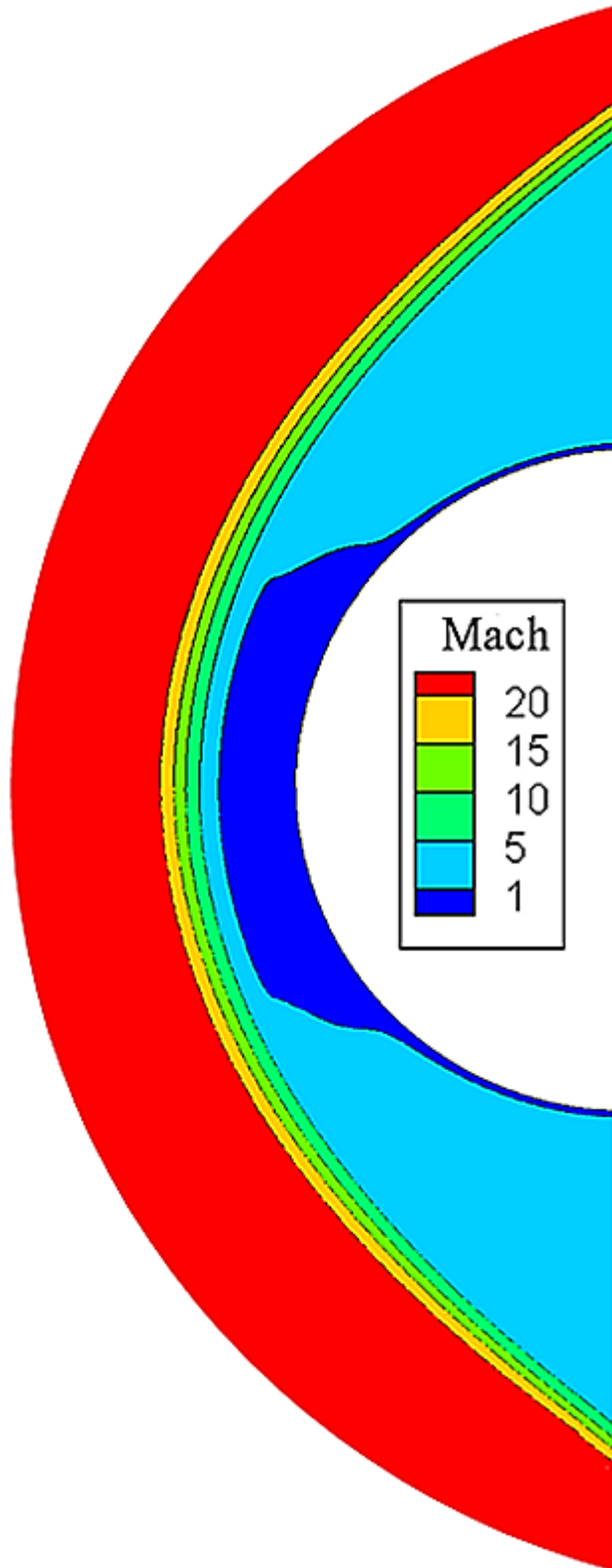
Figure 36 *Mach number contours predicted using dsmcFoam (Q-K) (lower half) and MONACO (TCE) (upper half) for reacting air flow over a 2D cylinder.*
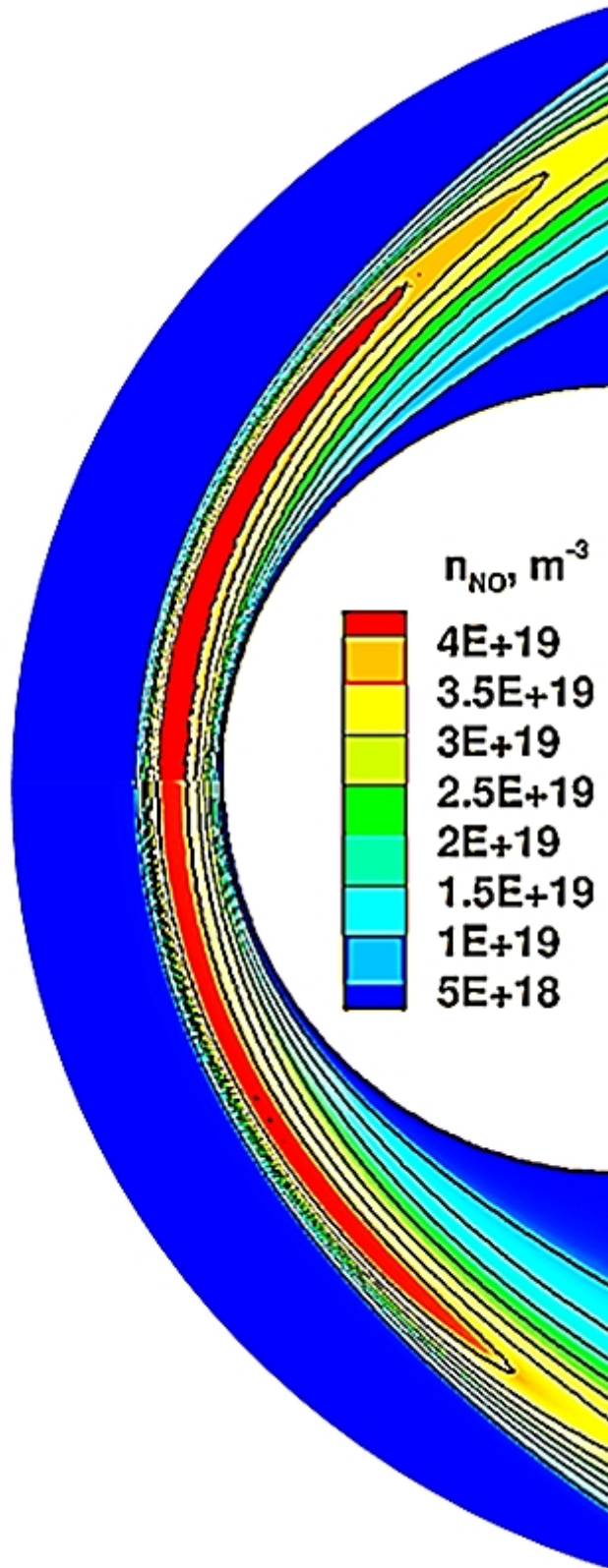
Figure 37 *Contours of NO predicted using dsmcFoam (Q-K) (lower half) and MONACO (TCE) (upper half) for reacting air flow over a 2D cylinder.*
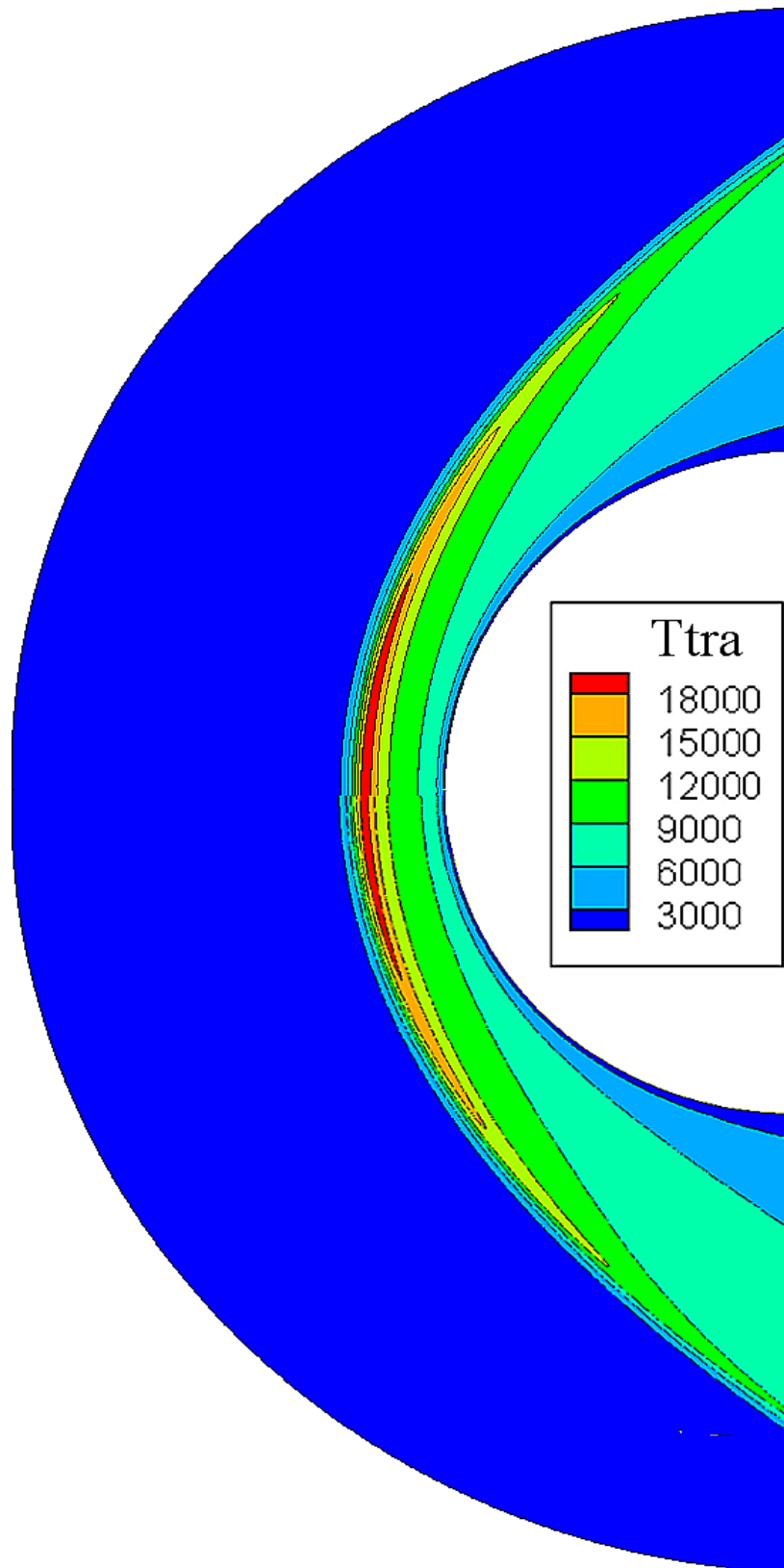
Figure 38 *Translational temperature contours predicted using dsmcFoam (Q-K) (lower half) and MONACO (TCE) (upper half) for reacting air flow over a 2D cylinder.*
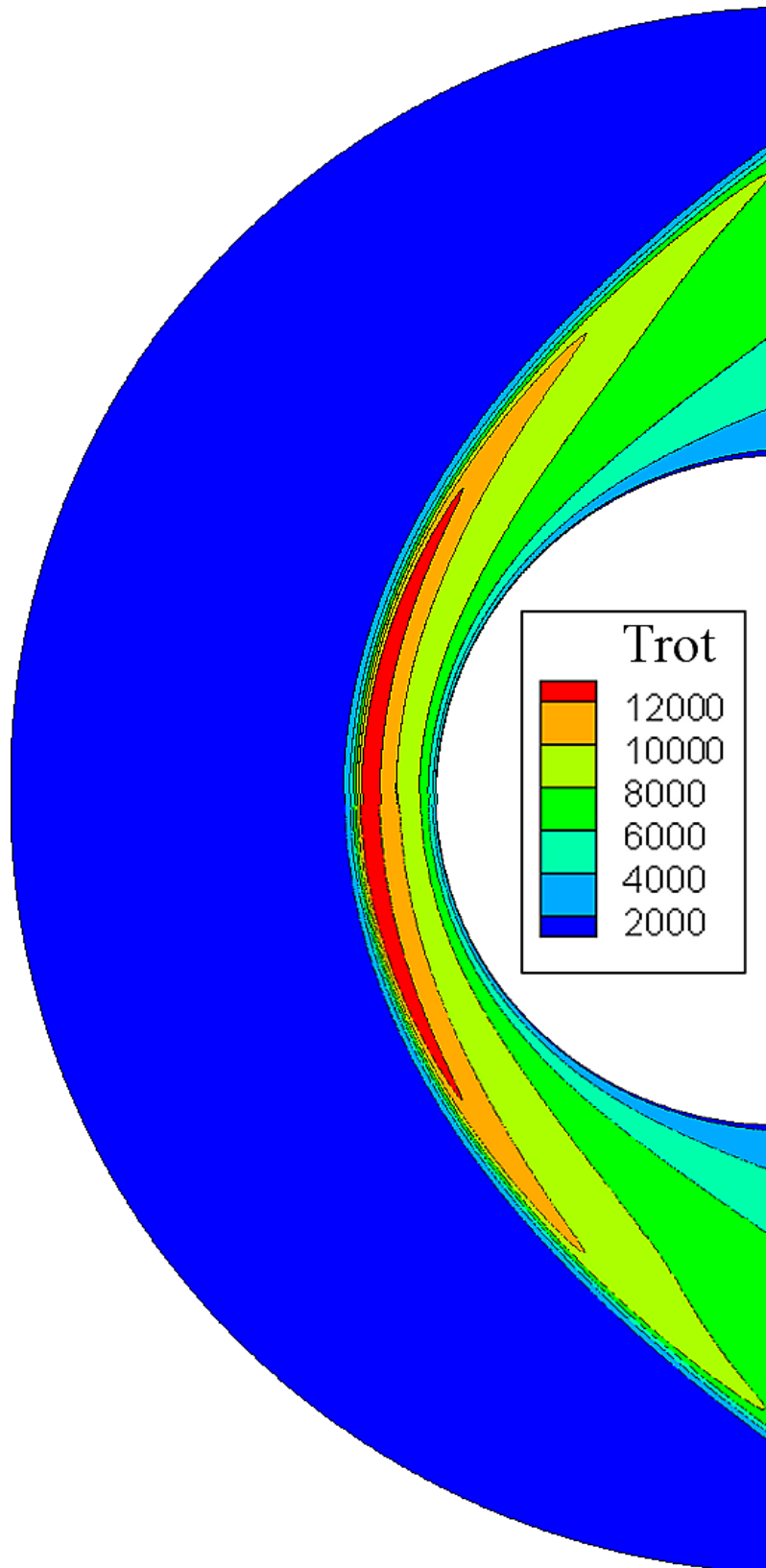
Figure 39 *Rotational temperature contours predicted using dsmcFoam (Q-K) (lower half) and MONACO (TCE) (upper half) for reacting air flow over a 2D cylinder.*
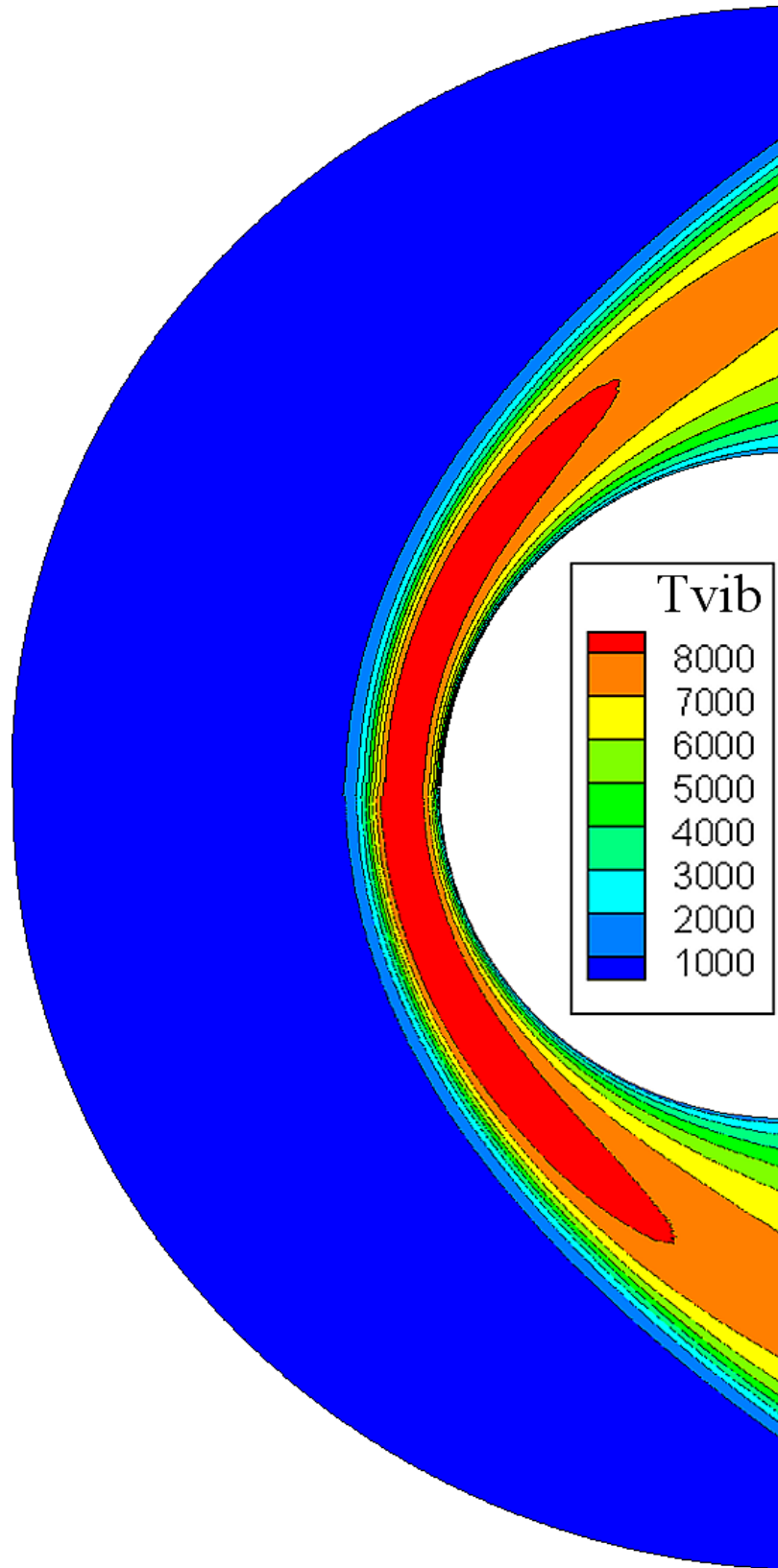
Figure 40 *Vibrational temperature contours predicted using dsmcFoam (Q-K) (lower half) and MONACO (TCE) (upper half) for reacting air flow over a 2D cylinder.*
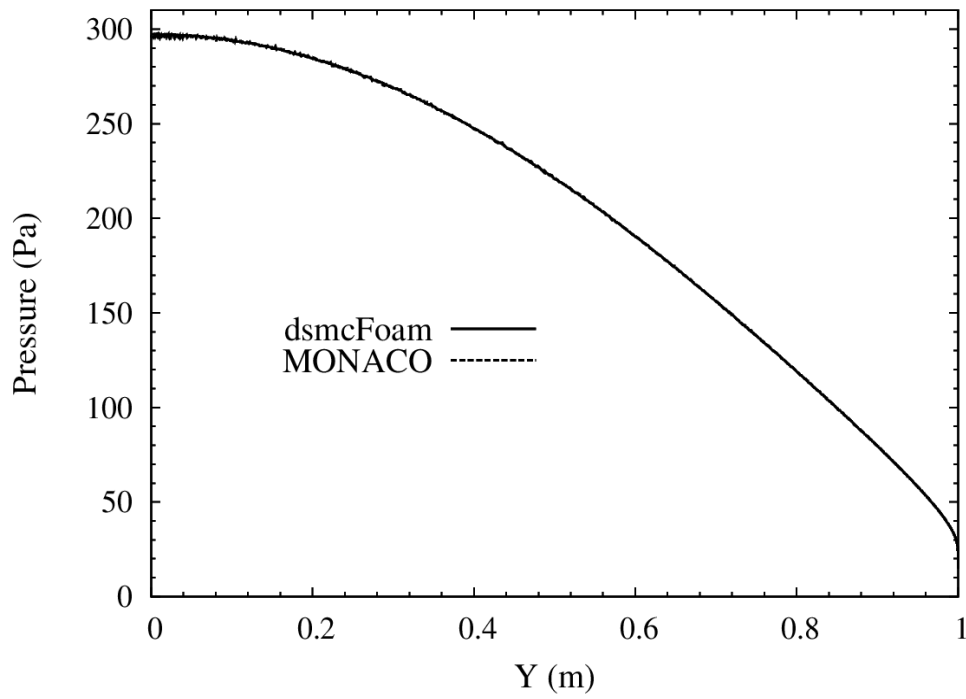
Figure 41 *Cylinder surface pressure for non-reacting flow. Y is the vertical position above the stagnation point.*
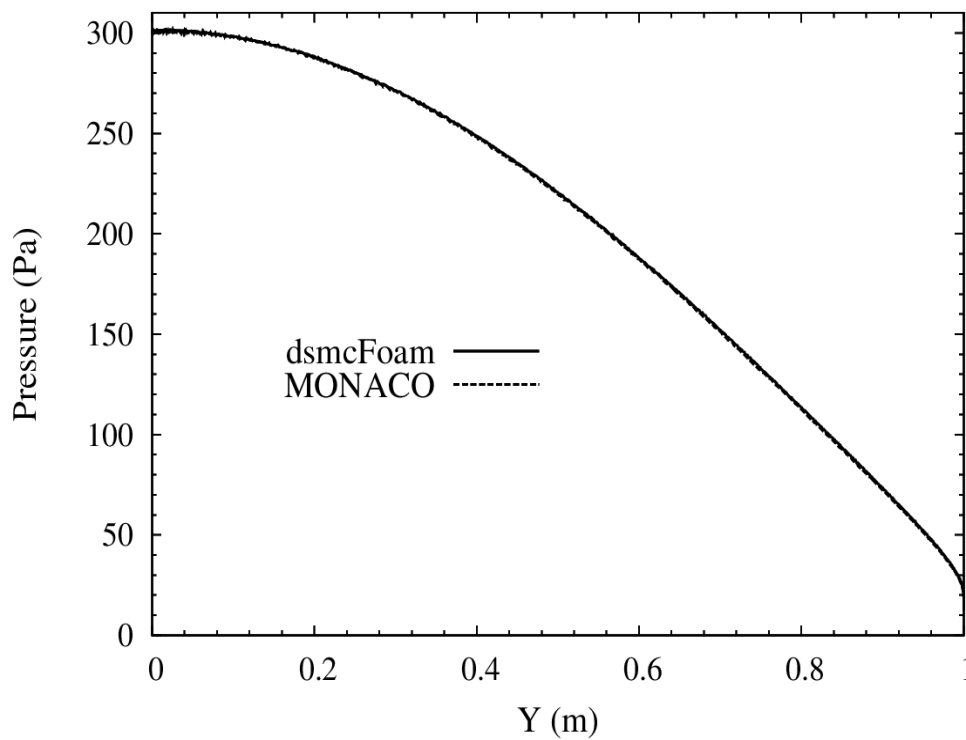
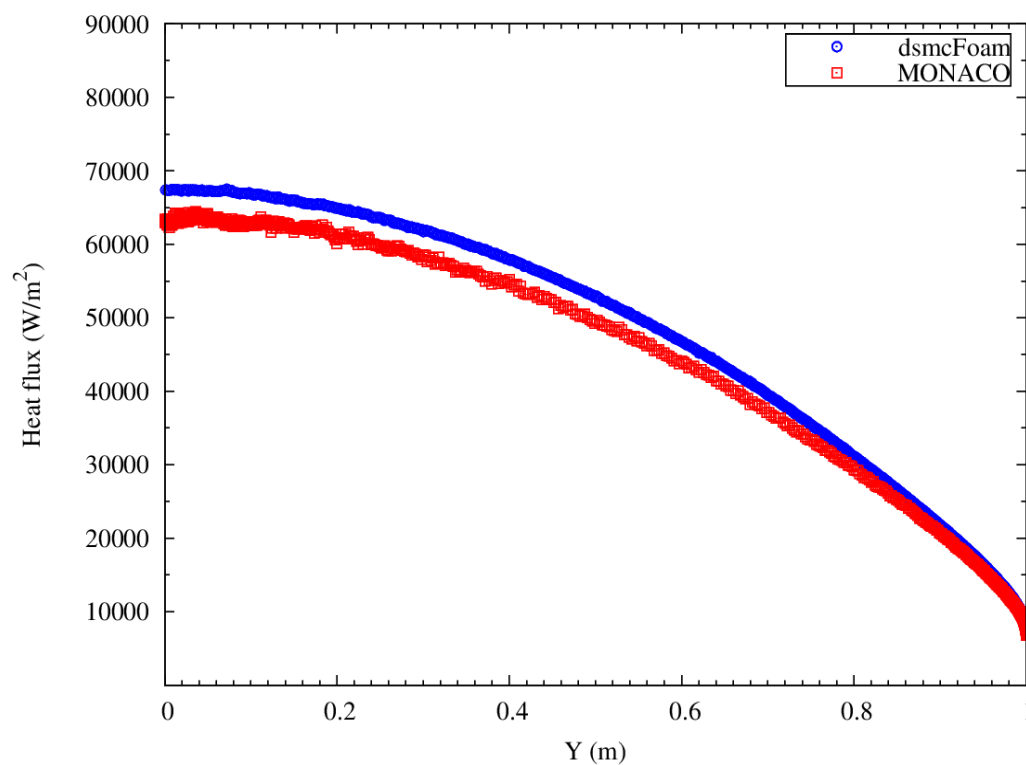**Figure 42** *Cylinder surface pressure for reacting flow. Y is the vertical position above the stagnation point.*
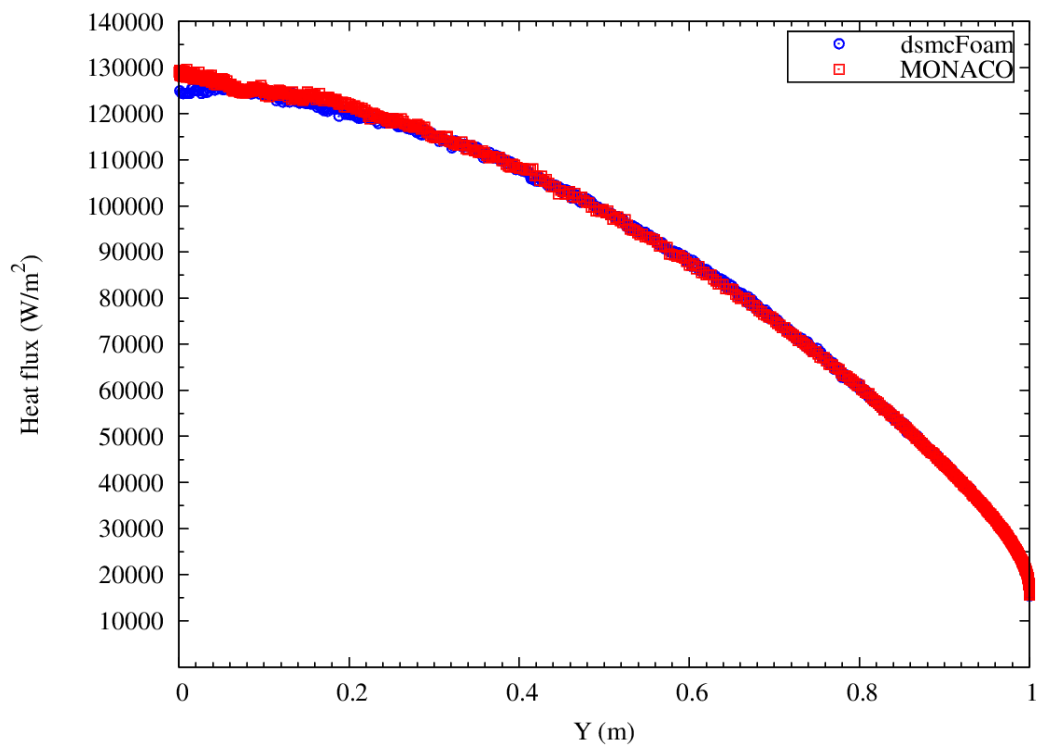
Figure 43 *Cylinder surface heat flux for non-reacting flow. Y is the vertical position above the stagnation point.*
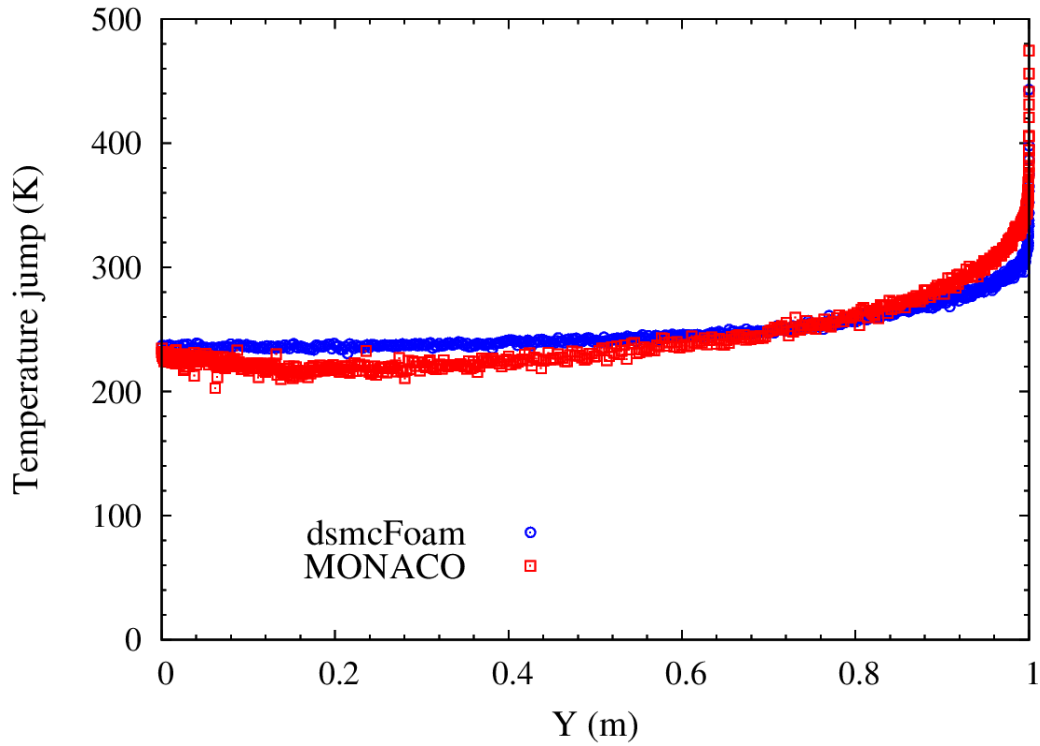

Figure 44 *Cylinder surface heat flux for reacting flow. Y is the vertical position above the stagnation point.*

Figure 45 *Cylinder surface temperature-jump for non-reacting flow. Y is the vertical position above the stagnation point.*
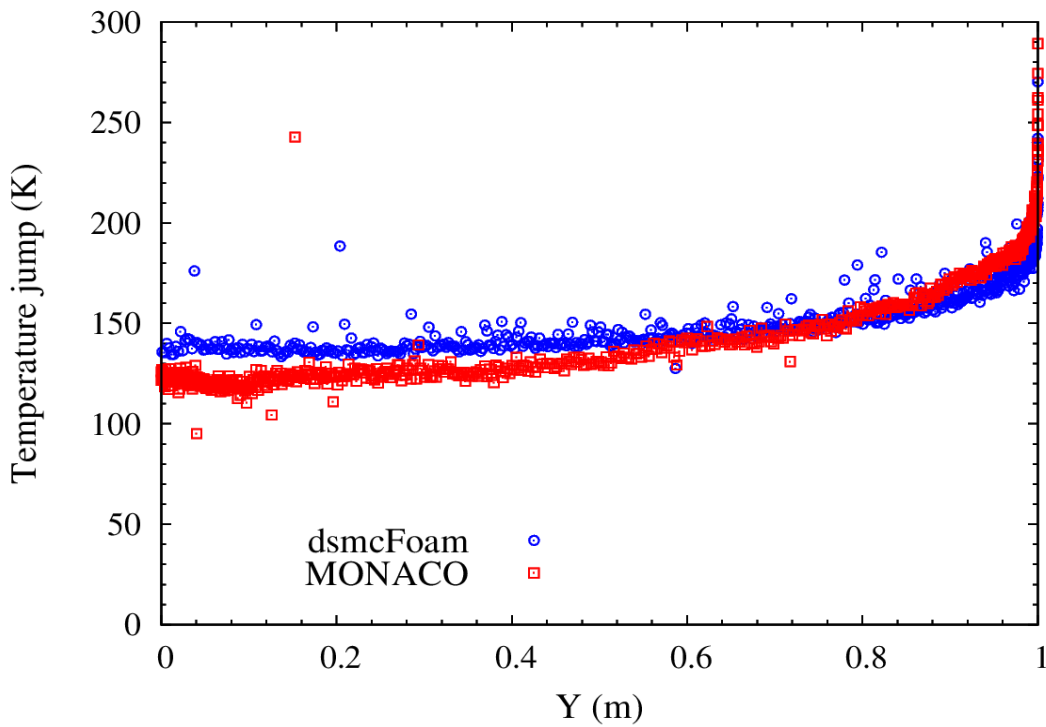

Figure 46 *Cylinder surface temperature-jump for reacting flow. Y is the vertical position above the stagnation point.*
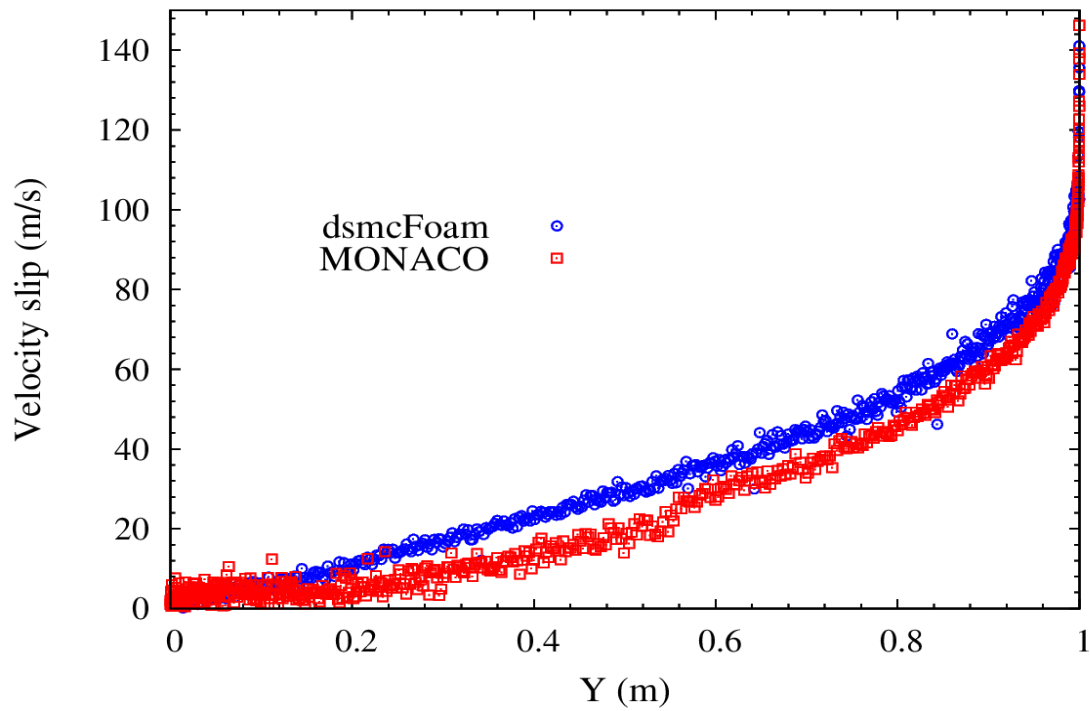
Figure 47 *Cylinder surface velocity-slip for non-reacting flow. Y is the vertical position above the stagnation point.*
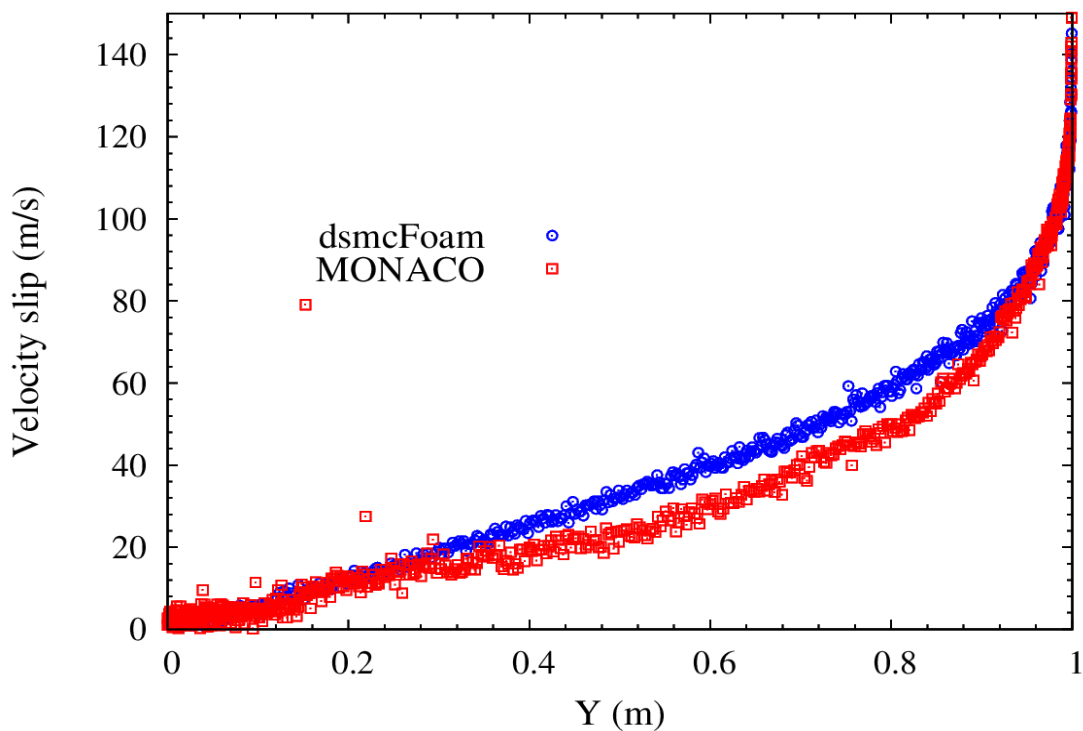

Figure 48 *Cylinder surface velocity-slip for reacting flow. Y is the vertical position above the stagnation point.*

References

[1]   Bird, G. A. The Q-K model for gas phase chemical reaction rates, *Phys. Fluids*, 23, 106101, 2011.

[2]   Gallis, M. A., Bond, R. B. and Torczynski, J.R. A kinetic-theory approach for computing chemical-reaction rates in upper-atmosphere hypersonic flows, *J. Chem. Phys.* 131, 124311, 2009.

[3]   Bertin, J. J. and Cummings, R. M. Critical hypersonic aerothermodynamic phenomena, *Ann. Rev. Fluid Mech.* 38:129-157, 2006.

[4]   Bhatnagar, P. L., Gross, E. P. and Krook, M. A model collision process in gases, *Phys. Rev.* 94: 511-525, 1954.

[5]   Yang, J. Y. and Huang, J. C. Rarefied flow computations using non-linear model Boltzmann equations, *J. Comp. Phys.,* 120(2): 323-339, 1995.

[6]   Greenshields, C. J. and Reese, J. M. The structure of shock waves as a test of Brenner's modifications to the Navier-Stokes equations, *J. Fluid Mech.*, 580: 407-429, 2007.

[7]   Bird, G.A. Molecular gas dynamics and the direct simulation of gas flows, Clarendon, Oxford, 1994.

[8]   Wagner, W. A convergence proof for Bird's direct simulation Monte Carlo method for the Boltzmann equation, *J. Stat. Phys.*, 66: 1011-44, 1992.

[9]   Anderson, J. D. Jr. Hypersonic and high temperature gas dynamics (second edition), McGraw-Hill, 2006.

[10]   http://www.openfoam.org

[11]   Scanlon, T. J., Roohi, E., White, C., Darbandi, M. and Reese, J. M. An open source, parallel, DSMC code for rarefied gas flows in arbitrary geometries. *Comput. Fluids*, 39, 2078-2089, 2010.

[12]   Haas, B. L., McDonald, J. D. and Dagum, L. Models of thermal relaxation mechanics for particle simulations, *J. Comp. Phys.*, 107(2): 348-358, 1993.

[13] Bergemann, F. and Boyd, I. D. New discrete vibrational energy model for the direct simulation Monte Carlo method. *Prog. in Astronaut. Aeronaut.*, 158: 174-183, 1994.

[14] Bird, G. A. A comparison of collision energy-based and temperature-based procedures in DSMC. *AIP Conference Proceedings*, 1084 (1): 245-250, 2008.

[15] Zuppardi, G., Morsa, L. and Romano, F. Influence of chemical models on the computation of thermo-fluid-dynamic parameters in hypersonic, rarefied flows. *Proc. I. of Mech. E., Part G*, 224: 637–646, 2010.

[16] Bird, G. A. *"Sophisticated DSMC"*, Notes prepared for short course at the DSMC07 meeting, 2007.

[17] Bird, G. A. Simulation of multi-dimensional and chemically reacting flows (past Space Shuttle orbiter), *Proc. 11th Int. Symp. Rarefied Gas Dynamics*, 365–388, 1979.

[18] I. D. Boyd. Modeling backward chemical rate processes in the direct simulation Monte Carlo method. *Phys. Fluids*, 19(12):126103, 2007.

[19] Wysong, I., Gimelshein, S., Gimelshein, N., McKeon, W. and Esposito, F., Reaction cross sections for two direct simulation Monte Carlo models: Accuracy and sensitivity analysis, *Phys. Fluids*, 24, 042002, 2012.

[20] Vincenti, W. G. and Kruger, C.H., *Introduction to Physical Gas Dynamics*, Wiley, New York, 1965.

[21] Haas, B. L. and McDonald, J. D., Validation of chemistry models employed in a particle simulation method, *J. Thermophys. Heat Transf.*, Vol. 7, No. 1, 1993.

[22] DSMC resources from Graeme Bird. *http://gab.com.au*, 2014.

[23] National Institute for Standards and Technology: http://kinetics.nist.gov/kinetics/kineticssearchform.jsp, 2014.

[24] Gupta, R. N., Yos, J. M., Thompson, R. A. and Lee, K. P. A review of reaction rates and thermodynamics and transport properties from an 11- species air model for chemical and thermal non-equilibrium calculation to 30,000 K, *NASA Reference Publication No. 1232*, NASA, Washington, DC, August

1990.

[25] Bortner, M. H. A review of rate constants of selected reactions of interest in re-entry flow fields in atmosphere, *U.S. Department of Commerce Report No. NBS TN 484*, 1969.

[26] Bird, G. A. The DSMC Method, Version 1.1, p.225. ISBN 9781492112907, 2013. www.createspace.com.

Acknowledgements